Biologically-Inspired Systems

Lars Heepe · Longjian Xue
Stanislav N. Gorb *Editors*

Bio-inspired Structured Adhesives

Biological Prototypes, Fabrication, Tribological Properties, Contact Mechanics, and Novel Concepts

Springer

Biologically-Inspired Systems

Volume 9

Series editor

Stanislav N. Gorb, Department of Functional Morphology and Biomechanics, Zoological Institute, Kiel University, Kiel, Germany

Motto: Structure and function of biological systems as inspiration for technical developments.

Throughout evolution, nature has constantly been called upon to act as an engineer in solving technical problems. Organisms have evolved an immense variety of shapes and structures from macro down to the nanoscale. Zoologists and botanists have collected a huge amount of information about the structure and functions of biological materials and systems. This information can be also utilized to mimic biological solutions in further technical developments. The most important feature of the evolution of biological systems is multiple origins of similar solutions in different lineages of living organisms. These examples should be the best candidates for biomimetics. This book series will deal with topics related to structure and function in biological systems and show how knowledge from biology can be used for technical developments in engineering and materials science. It is intended to accelerate interdisciplinary research on biological functional systems and to promote technical developments. Documenting of the advances in the field will be important for fellow scientists, students, public officials, and for the public in general. Each of the books in this series is expected to provide a comprehensive, authoritative synthesis of the topic.

More information about this series at http://www.springer.com/series/8430

Lars Heepe · Longjian Xue
Stanislav N. Gorb
Editors

Bio-inspired Structured Adhesives

Biological Prototypes, Fabrication, Tribological Properties, Contact Mechanics, and Novel Concepts

Springer

Editors
Lars Heepe
Department of Functional Morphology
and Biomechanics, Zoological Institute
Kiel University
Kiel
Germany

Stanislav N. Gorb
Department of Functional Morphology
and Biomechanics, Zoological Institute
Kiel University
Kiel
Germany

Longjian Xue
School of Power and Mechanical Engineering
Wuhan University
Wuhan
China

ISSN 2211-0593 ISSN 2211-0607 (electronic)
Biologically-Inspired Systems
ISBN 978-3-319-59113-1 ISBN 978-3-319-59114-8 (eBook)
DOI 10.1007/978-3-319-59114-8

Library of Congress Control Number: 2017943120

This Springer imprint is published by Springer Nature
The registered company is Springer International Publishing AG
The registered company address is: Gewerbestrasse 11, 6330 Cham, Switzerland

This book is dedicated to the memory of Dr. Uwe Hiller (Münster University, Germany), the pioneer of ultrastructural and experimental works on gecko adhesion

Chapter 15
On the Bioadhesive Properties of Silicone-Based Coatings by Incorporation of Block Copolymers

Thị Chinh Ngo, Radostina Kalinova, Rosica Mincheva, Audrey Beaussart, Elise Hennebert, Patrick Flammang, Yves Dufrêne, Philippe Dubois, Roberto Lazzaroni and Philippe Leclère

Abstract This chapter discusses the applicability of different AFM-based techniques with force sensitivity of a few pN for mapping the nanostructure and quantifying the nanoscale mechanical properties of the surface of complex polymer coatings based on silicone oligomers in order to use them as bioadhesives. The AFM modes used are Peak Force Tapping and Contact with Si_3N_4 and chemically-modified (CH_3-terminated alkanethiols, COOH-terminated alkanethiols) probe tips both in air and aqueous media. Studying nanostructured films of

T.C. Ngo · R. Lazzaroni · P. Leclère (✉)
Laboratory for Chemistry of Novel Materials, Center of Innovation and Research in Materials and Polymers (CIRMAP), Research, Institute for Materials Science and Engineering, University of Mons (UMONS), 20 Place du Parc, 7000 Mons, Belgium
e-mail: Philippe.Leclere@umons.ac.be

R. Lazzaroni
e-mail: Roberto.Lazzaroni@umons.ac.be

Present Address:
T.C. Ngo
Institute of Research and Development, Duy Tan University, K7/25 Quang Trung, Da Nang, Vietnam

R. Kalinova · R. Mincheva · P. Dubois
Laboratory of Polymeric and Composite Materials, Center of Innovation and Research in Materials and Polymers (CIRMAP), Research, Institute for Materials Science and Engineering University of Mons (UMONS), 20 Place du Parc, 7000 Mons, Belgium
e-mail: rosica.mincheva@umons.ac.be

P. Dubois
e-mail: Philippe.Dubois@umons.ac.be

Present Address:
R. Kalinova
Institute of Polymers, Bulgarian Academy of Science, Acad. G. Bonchev Str., Block 103-a, 1113 Sofia, Bulgaria

L. Heepe et al. (eds.), *Bio-inspired Structured Adhesives*,
Biologically-Inspired Systems 9, DOI 10.1007/978-3-319-59114-8_15

block copolymers containing a polydimethylsiloxane (PDMS) segment and a segment of poly(acrylic acid) (PAA) or poly[(2-dimethylamino) ethyl methacrylate] (PDMAEMA) led to a better understanding of the interaction of the polymer chains with solvent molecules or chains of another polymer in the self-assembly process. Stiffness mapping by PFT-AFM has allowed identifying the difference in mechanical properties between two polymer constituting blocks. The effect of copolymer concentration and solvents on the surface morphologies was also studied in details. In more complicated situation, the copolymers were used to modify the surface properties of elastomeric PDMS coatings and the PDMS surface properties before and after immersion in water were also evaluated. AFM-based nano-mechanical testing showed that the surface reorganization significantly affects the morphology and the adhesion properties of the silicone coatings. The observed broadening of the adhesion distribution is believed due to the different interactions between hydrophobic/hydrophilic surfaces and the silicon probe tip in aqueous solution. Finally, the nature of the tip-surface interaction forces was clarified by employing functionalized AFM tips. The adhesion force mapping with hydrophobic tips (CH_3-terminated alkanethiols) for 10 wt% PDMS-*b*-PDMAEMA-filled coatings before and after immersion in water showed larger forces for the coatings before immersion, thus confirming that the interaction forces between two hydrophobic surfaces are stronger than those between one hydrophobic and one hydrophilic surface. In addition, the interaction forces between amino groups of the PDMAEMA and COOH-terminated tips were investigated as a function of the pH and the ionic strength of aqueous media. Progressive stretching and continuous desorption of individual copolymer chains from the tip surface were recorded. The dynamic changes of polymer desorption were also reported by recording force curves at various pulling speeds and contact times. Furthermore, the adhesion force maps recorded at high ionic strength (in 0.1 M NaCl solution) showed a major decrease in the adhesion frequency and plateau forces, indicating a loss of polyelectrolyte properties. Bio-adhesion experiments with mussels were then performed

A. Beaussart · Y. Dufrêne
Biochemistry, Biophysics and Genetics of Microorganisms (BBGM), Université catholique de Louvain (UCL), Croix du Sud 1, 1348 Louvain-la-Neuve, Belgium
e-mail: audrey.beaussart@uclouvain.be

Y. Dufrêne
e-mail: yves.dufrene@uclouvain.be

Present Address:
A. Beaussart
Laboratoire Interdisciplinaire des Environments Continentaux, UMR 7360 CNRS—Université de Lorraine, 15 Avenue du Charmois, 54500 Vandoeuvre-les-Nancy, France

E. Hennebert · P. Flammang
Laboratoire de Biologie Marine, Research Institute for Biosciences, University of Mons (UMONS), 20 Place du Parc, 7000 Mons, Belgium
e-mail: Patrick.Flammang@umons.ac.be

on the different types of substrates—unfilled PDMS coatings and PDMS coatings filled with block copolymers. The results revealed that these organisms attach preferably to block copolymer-filled coatings after immersion due concomitant molecular reorganization at the top-surface of the copolymer-filled coatings. These observations provided evidence for the significant role played by the selected amphiphilic block copolymers to promote bio-adhesion on surface-treated silicone coatings.

15.1 Introduction

Polymers have found applications in different areas as molds, foils, thin films, coatings, adhesives, joints, blends, composites as well as biomaterials, they have been also used in micro- and nanotechnology. The surfaces and interfaces of polymer materials have strong influence on their properties (such as adhesion, friction, wetting, swelling, penetrability and biological compatibility). Particularly, block copolymers occupy a large area of research due to their well-controlled molecular architecture and chemical composition. Those copolymers especially exhibit the combined properties of different components that offer widespread applications in industry as well as daily-life. Among all copolymers, amphiphilic block copolymers are one of most interesting classes of synthetic systems for creating self-assembled nanostructures [1–3].

Among all polymers, polydimethylsiloxane is of great particular interest. Particularly, the cross-linked PDMS called silicone rubber or silicone elastomer has demonstrated a long history of use in multiscale structured surfaces [4]. PDMS has also been widely used for a number of biotechnological, biomedical applications due to its extraordinary features (such as excellent flexibility, nontoxicity, easy sealing with other materials, oxidative stability, and relatively low temperature of curing) [5–7].

PDMS possess extremely high flexibility and high mobility of polymer chains compared to other polymers, which in fact directly correlates with the very low value of its glass transition temperature ($T_g^{PDMS} \sim -125$ °C). The flexibility of PDMS chains can result in two different conformations by exposing either methyl groups or oxygen atoms outwards at the polymer surface. In air the apolar methyl groups point outwards and occupy the surface of PDMS, which leads to hydrophobicity (Fig. 15.3a). In contact with water, because the chains are very flexible and mobile, they can restructure to expose the polar oxygen groups to the PDMS/water interface as shown in Fig. 15.1.

PDMS is also water impermeable and has long time durability in the presence of aqueous solutions [8], which is an important requirement for its possible use as underwater adhesive. However, its application range is somehow restricted by the risk of adhesion failure due to its low surface free energy (19.9 mJ/m^2) and extremely low chemical reactivity [8, 9] This can be overcome by increasing the

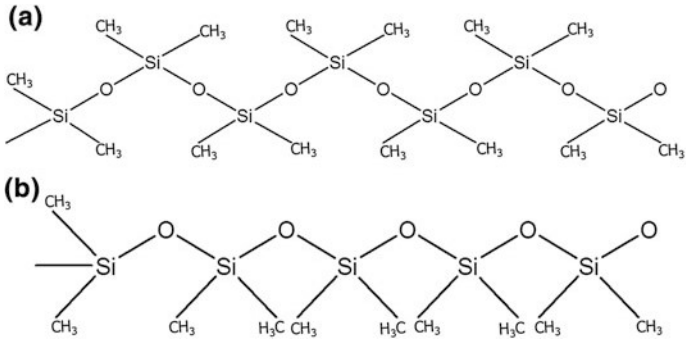

Fig. 15.1 Schematic representations showing the two possible orientations of PDMS chains

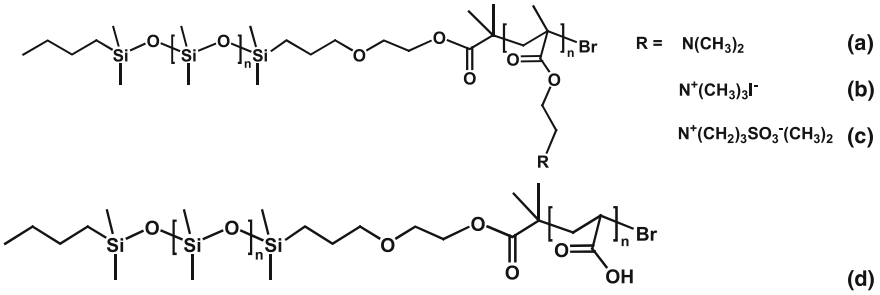

Fig. 15.2 Chemical structures of **a** polydimethylsiloxane-*b*-poly-[(2-dimethylamino) ethyl methacrylate], **b** polydimethylsiloxane-*b*-poly[(quaternized 2-dimethylamino) ethyl methacrylate], **c** polydimethylsiloxane-*b*-poly[(betainizied 2-dimethylamino) ethyl methacrylate], **d** polydimethylsiloxane-*b*-poly(acrylic acid)

PDMS surface energy and reactivity via introduction of reactive functional groups at the polymer surface. The functionalization of polymer surfaces is usually achieved by using physical or chemical processes (like plasma treatment or surface grafting) or a combination of both [10]. These techniques are able to improve the hydrophilicity of the PDMS surface without affecting its properties.

In our study, amphiphilic poly(dimethylsiloxane)-*b*-poly-[(2-dimethylamino) ethyl methacrylate] (PDMS-*b*-PDMAEMA) bearing pendent tertiary amine groups along the poly(methacrylate) block (Fig. 15.2a), and polydimethylsiloxane-*b*-poly (acrylic acid) (PDMS-*b*-PAA) bearing carboxylic groups along the poly (acrylate) sequence (Fig. 15.2d), were synthesized through atom transfer radical polymerization (ATRP). Then, in order to study the charge-type/adhesion relationship, modified PDMS-*b*-PDMAEMA was obtained by quaternization (introduction of quaternary amines, Fig. 15.2b) and betainization (introduction of zwitterions, Fig. 15.2c) reactions of the tertiary amine functions [11].

The development of scanning probe techniques plays an important role for the progress of nano-science and nanotechnology [12]. In particular, Atomic Force

Microscopy (AFM) has been used to investigate a wide range of materials (conductive, semi-conductive, insulating, ceramics, polymers, …), including soft biological systems (proteins, membranes, living cells…) [13–15] in multiple environments (air, UHV, liquid, electrochemical…). AFM is also well known as an appropriate technique to visualize the microstructure, combined with the probing of the nano- and micro-mechanical properties of material surface at the nanoscale [16].

In order to estimate the mechanical properties of a sample by AFM, a sharp probe has to establish a stable contact with the sample surface. The system usually consists of a flexible cantilever with a sharp, microfabricated probe at its end which can eventually chemically modified in order to measure local forces. In this later case, the technique is called "Chemical Force Microscopy (CFM)" [17]. Typically, these cantilevers are rectangular or V-shaped, besides other shapes of cantilevers exist for some specific applications [18]. Cantilevers are usually made of single crystal silicon of silicon nitride. The back side (opposite to the tip side) of the cantilever is generally coated with a thin metal layer (gold, platinum, or aluminum) to improve the reflectivity of the cantilever when the laser spot coming from a laser diode is back reflected into a four-quadrant photodiode. This method is the most commonly used and is named "optical lever detection". By using this kind of photodiode, it is very easy to separate the contributions of vertical and horizontal deflections of the cantilever to determine the topography and the friction properties, respectively. The sensitivity of the photodetector to the applied (low) forces depends on the shape and spring constant of the cantilever, which may vary from 0.01 to 100 N/m.

To obtain the mechanical properties, the data acquisition can occur either in the "quasi-static" or "dynamic mode". Historically, and because of the easiness of the technique, the first developed mode for the mechanical measurements involved quasi-static loading of the sample surface. In this mode, the AFM tip is brought into contact with the sample surface, pressed against it, and after withdrawn. This full approach-retract cycle is then able to provide the so-called "force-distance curve (FD curve)" by calculating the forces from the tip deflection against the piezo actuator position. Applications of various contact mechanics models to fit this FD curves allow for the calculation of the main mechanical properties at the nanometer scale such as the elastic modulus, the sample deformation, and the adhesion [16, 19]. Among the most commonly used models, depending on the applications (mainly driven by the softness and the adhesion of the sample), one can consider Derjaguin–Muller–Toporov (DMT) [20], Johnson–Kendall–Robert (JKR) [21], or other more sophisticated models [22].

AFM visualization of the mechanical properties in each pixel of the image is frequently called "Force-Volume (FV)" imaging mode. This mode if the mechanical model is appropriately chosen allows to provide the quantitative mapping of the regions of different mechanical behavior on the nanoscale and has been used to characterize many polymeric systems. Despite its usefulness of this important mode, there are however several pitfalls to this technique. The first one is related to the assumptions of chosen contact mechanics model. These contact mechanics models are usually applied for simple indenter shapes (such as paraboloid, sphere,

cone, and pyramid), and the nanoscale dimensions of AFM-based measurement can strongly influence the calculated elastic properties. Thus, this is important to note that to perform quantitative calculations, the tip shape should be precisely characterized [for instance by Scanning Electron Microscopy (SEM)]. The fact that the simple contact mechanics models is ideally flat sample topography in also an important assumption. Another issue to carefully consider for the FV mapping is related to the fact that a single measurement is performed at a constant indentation rate and this rate is limited by the nonlinearities of piezo-actuator extension [23]. The FV mode is very time consuming which is a last but not least drawback. Even if "Fast Force Volume" mode has been recently introduced [24], in order to overcome these drawbacks, dynamic measurement modes were developed.

In dynamic methods, high frequency vibrations are applied to the tip–sample contact through the actuation of the cantilever, the sample, or both. Among them, Tapping Mode is the most famous [25]. Typically, Tapping Mode AFM is performed in "amplitude modulation" mode: the height of the cantilever position is constantly adjusted to keep a constant ratio of the tip vibrational amplitude in contact with the sample surface to its oscillation amplitude in air, thus imaging topographical features of the sample. The phase shift of the vibrations relative to the excitation vibrations bears information about the energy dissipation by the tip into the sample. The phase imaging technique can be used to produce excellent material contrast, especially in systems with close mechanical properties, without any additional post processing of the measurement data. Due to the fact that forces existing between the surface and the tip are not directly measured in TM-AFM, this technique does not allow for quantitative measurements of the elastic modulus of the material. However, it was shown since more than two decades that it can be used to perform contrast variation in some cases [26].

In contrast to TM-AFM, Force Modulation Microscopy measurement (FMM) is performed in contact mode. The cantilever is vertically displaced to maintain constant deflection while the tip is imaging the surface, while at the same time the cantilever is vibrated at a frequency much lower than the resonance frequency [27]. In Contact Resonance AFM (CR-AFM), similar to the FMM, scanning is also performed in the contact mode and cantilever is dynamically excited at high frequency range at relatively low amplitude. However, in CR-AFM vibrations of the tip are kept close to the resonance frequency of the cantilever, which is not the case for FMM [28]. With these two modes, the relative Young modulus can be acquired as well by using a calibration sample with well-known elastic properties. This calibration process has to be done for each new experiment which can be rapidly fastidious. Anyway, the simplest way is to perform qualitative imaging by CR-AFM, which is executed by keeping the vibration frequency constant and monitoring the change in amplitude as the tip scans the sample. The contrast of the image can be tuned by the changes of the oscillation frequencies around the resonance peak or by switching to different vibrational modes [29]. To be complete, another mode of operation of CR-AFM is a spectroscopic mode. In this mode, the vibration amplitude is recorded for the range of vibrational frequencies, establishing the full shape of the resonance curve at each point. Knowing the resonance

frequency allows one to apply analysis similar to the one in the FMM method to calculate stiffness of the tip–sample contact [30]. In CR-AFM, it is also possible to track the position of the resonance peak by keeping the frequency window close to each previous resonance position for each subsequent point [31]. Once again, this method is time consuming and is better applicable to stiff samples. Therefore, several improved methods have been proposed such as 'Dual AC resonance tracking (DART) where two separate frequencies are applied to the vibrating cantilever [32]. *In fine*, the "ultrasonic AFM (UAFM)" technique is similar to FMM and CR-AFM in that the tip is constantly pressed against the sample surface and the vibrations are induced into the tip–sample contact with the applied frequency much higher than the natural resonance of the cantilever and the amplitude of this frequency is constantly changing, while the average tip deflection is monitored [33].

Pulsed Force (PF) modes have also to be consider if the quantitative mapping of the mechanical properties is needed. Firstly introduced by Marti [34] in 1997, the methodology has been declined by many manufacturers or laboratories and even the principle is basically the same, PF is nowadays known with different names such as PeakForce Tapping (PFT) [35], Intermittent Contact Resonance AFM [36], Digital Pulsed Force Microscopy [37], HybriD mode [38], Quantitative Imaging (QI) AFM [39], PinPoint Mode [40], Ringing Mode [41], … . In PF, each measurement cycle (corresponding to one pixel of the image) starts above the surface, then the tip approaches and makes a very brief contact with the surface resulting in a small indentation. The depth of the indentation of the tip is controlled by the maximum force exerted on the sample by the cantilever (set point). The cycle is finalized by withdrawing the tip from the surface up to the initial baseline static deflection. By limiting the set point from few nN to few pN (depending on the sample stiffness), indentations as small as 1–2 nm can be performed, therefore very soft, nondestructive measurement conditions could be achieved.

Recently, multifrequency techniques have been proposed and seem very promising if one can adapt the most appropriate model(s) to the recorded raw data and is able to reconstruct the force distance curves closer to the actual ones. To name a few here, we can cite: HarmoniX^{TM} [42], Band Excitation AFM [43], Intermodulation AFM [44], mode-synthesizing atomic force microscopy [45], G-mode AFM [46], …

Since it appears that the mechanical properties of a sample surface can be determined by different AFM techniques that depends on the way that the measurement is done aiming at the correct or the most accurate description of the tip-surface interactions, in this work we deliberately focused on two of them, namely Chemical Force Microscopy and Peak Force Tapping (PFT). PFT is a recent technique that allows simultaneously the recording of data on the topographic profile (i.e., the surface morphology) and the surface nano-mechanical properties with high resolution in different media including water. This is more difficult to quantitatively provide these properties with the other scanning probe techniques described above (mainly for tip and detector calibrations which are mandatory to provide quantitative measurements). This technique gives a number of advantages compared to other modes. PFT-AFM operates at a frequency of

approximately 2 kHz, the time required for obtaining high-resolution images of those properties is less than that in the case with approach-retract curves recorded at 1 Hz. PFT can generate mechanical maps at higher resolution (up to 2048 pixels × 2048 pixels) compared to 64 pixels × 64 pixels at best in Force-Volume imaging. Contact-mode topographic image and FV-adhesion map are recorded separately while PFT provides simultaneously topographic and mechanical images with high resolution and relatively high-speed imaging.

In addition, Peak Force operation offers the benefits of both contact and Tapping mode: one can not only control constantly the force between the tip and the sample but also minimize the lateral forces by intermittently contacting the sample. Therefore, it is possible to minimize damages for the tip and the studied sample, which is of great interest for imaging of soft and delicate biological materials. PFT operates in a non-resonant mode and at low force; this is particularly advantageous in liquids. Using V-shaped silicon nitride probes with a low spring constant (less than 1 N m^{-1}), PFT-AFM gives higher force sensitivity compared to Tapping mode. The cantilever stiffness will be chosen based on the sample stiffness in order to cause enough deformation of the sample and still retain high force sensitivity. The probe is calibrated on a hard and clean surface prior to the experiment, in order to directly quantify the force as well as the mechanical properties.

In our study, the morphology and microstructure of PDMS-*b*-PAA and PDMS-*b*-PDMAEMA block copolymer thin films and their adhesion properties were firstly investigated using Atomic Force Microscopy. Depending on the copolymer structure, chemical composition and on the nature of the solvent, a variety of morphologies were obtained through the self-assembly of the block copolymer chains. These four copolymers were then in a second step used for modifying the surface properties of elastomeric PDMS coatings. The idea is to achieve a reversible adhesion between the ionic segments of the amphiphilic block copolymers incorporated in silicone coatings in aqueous media as a function of specific and controllable conditions (pH, ionic strength, temperature) interactions (as shown in Fig. 15.3).

In this context, the surface restructuring of PDMS in water was investigated by Chen et al. [47] using sum frequency generation (SFG) vibrational spectroscopy. The results showed that the methyl groups of PDMS tilt more toward the surface upon contact with water. Beigbeder et al. [48] also demonstrated some decrease in the surface hydrophobicity when PDMS chains get in contact with water. This is

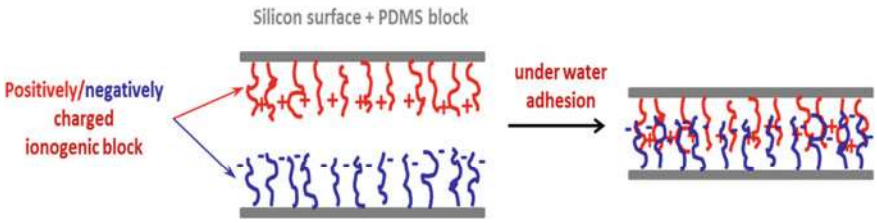

Fig. 15.3 Schematic representation of reversible adhesive in aqueous media

suggested to be a consequence of the reorganization of the siloxane backbone and the methyl groups at the coating surface. In order to functionalized PDMS coatings, many approaches have been proposed and most of them are described in the recent review by Kalinova et al. [49].

More recently, the addition of copolymers to PDMS has been proposed as a valuable pathway to tune the anti-fouling properties of silicone. Martinelli et al. [50, 51] have prepared coatings by blending amphiphilic copolymers containing poly (ethylene glycol) (PEG)-fluoroalkyl acrylate and polysiloxane methacrylate with a PDMS matrix in order to investigate the effect of the copolymer on the biological performance. The results of the immersion tests showed a better performance towards hard fouling for coatings containing the amphiphilic copolymer, compared to those without copolymer. AFM analyses showed the changes in the surface morphology of the coatings after immersion, possibly due to the swelling of the PEGylated portions at the surface [50].

Several techniques were used to evaluate the effect of the block copolymer on the PDMS surface properties before and after immersion in water. Contact angle measurements served to measure surface wettability. X-ray photoelectron spectroscopy (XPS) was then used in order to determine the surface chemical composition. Peak Force Tapping AFM and Chemical Force Microscopy were applied to investigate the surface morphology and to quantitatively measure the adhesion on the nanoscale. Finally, the bio-adhesion properties were tested by experiments with mussels, a major biological model for underwater adhesion [52–54].

15.2 Self-assembly of PDMS-Based Block Copolymers

In the case of diblock copolymers, depending on their structure, chemical composition and used solvent, a variety of morphologies can be obtained. It is known that if both block components exhibit similar solubility parameters, they are soluble in the same solvents. Repulsion between the blocks leads to different morphologies that are thermodynamically driven [55]. In contrast, a variety of self-assembled aggregates called micelles can be formed in dilute solution when the solvent preferentially solvates one of the blocks.

As already known in the literature, the strength of polymer-solvent interaction is crucially related to the solvent quality which is commonly assessed by the Hildebrand solubility parameter (δ) [56]. According to this approach, a good solvent must have a very similar solubility parameter to that of the polymers. Based on the solubility parameters presented in Table 15.1, one can conclude that THF is a selective solvent for PDMS and PDMAEMA blocks while the PAA blocks are better soluble in MeOH.

In this study, two block copolymers including PDMS-*b*-PDMAEMA (M_n^{PDMS} = 10,000, $M_n^{PDMAEMA}$ = 15,600) and PDMS-*b*-PAA (M_n^{PDMS} = 10,000, M_n^{PAA} = 12,100) were dissolved in THF and a mixture of THF and MeOH, respectively, at

Table 15.1 Solubility parameters for the solvents and the block copolymer components [89–91]

Solvent or polymer	Solubility parameter δ $(MPa)^{1/2}$
THF	18.5
MeOH	29.7
THF/MeOH	24.9
PDMS	14.6
PAA	24.6
PDMAEMA	18.8

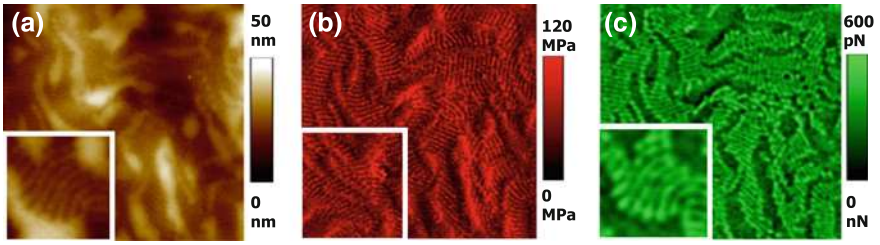

Fig. 15.4 PFT-AFM images (2 μm × 2 μm and a zoom 400 nm × 400 nm) of a PDMS-*b*-PDMAEMA block copolymer thin film obtained from a 0.1 g/mL copolymer/THF solution (M_n^{PDMS} = 10,000, $M_n^{PDMAEMA}$ = 15,600). **a** Height; **b** stiffness; **c** adhesion

concentration of 0.1 g/mL. The films were then prepared by spin coating at 4000 rpm for 120 s. The desired films are formed after the evaporation of the solvent. AFM measurements were performed in Peak Force Tapping with a Dimension Icon in air and in ambient conditions. V-shaped silicon nitride probes (k ∼ 0.3–0.4 N m^{-1}) cantilever were used. The oscillation of the probe tip was operated in the vertical direction at a frequency of approximately 2 kHz. The probe was calibrated on a stiff surface prior to the experiments, in order to quantify the tip-sample forces. All images were digitally recorded with a resolution of 512 pixels/line. The scan rate was kept at 0.5 Hz. The Nanoscope image processing software was used for image analysis.

15.2.1 Self-assembly of PDMS-b-PDMAEMA Copolymers in THF Non-selective Solvent

Figure 15.4a–c, respectively displays topographic, elastic modulus and adhesion images obtained simultaneously on the same area of the surface for a PDMS-*b*-PDMAEMA copolymer film. The topographic image shows a lamellar morphology consisting of alternating stripes of the polymer components.

The Young modulus derived by using the DMT model (vide supra) mapping shows the alternation of dark and bright stripes (Fig. 15.4b) accounting for the different stiffness of the constituent polymer components. The darker domains are

considered to be the softer PDMS (stripe width: 14 nm), while the brighter areas correspond to lamellae of stiffer PDMAEMA (stripe width: 26 nm). In parallel, the adhesion image (Fig. 15.4c) demonstrates that the stiffer PDMAEMA regions are less adhesive (darker stripes in the adhesion image) than the softer PDMS (brighter stripes in the adhesion image). These data correlate well with observations on the modulus map, since it is easier for the AFM tip to separate from a harder surface than from a softer one.

15.2.2 Self Assembly of PDMS-b-PAA Block Copolymers

PFT images presented in Fig. 15.5 illustrate a spherical morphology. The aggregation size is 50 ± 4 nm. The formation of spherical aggregations is the result of the micro-phase separation of block copolymers in selective solvents [57]. Depending on the solvent quality and solubility parameter (δ) [56, 58, 59], the micelle-like aggregates can be formed as a result of the association of the insoluble blocks [60–62].

In this case, the solubility parameter of the PAA (δ = 24.6 $MPa^{1/2}$) is almost the same to one of THF/MeOH mixture (δ = 24.9 $MPa^{1/2}$) (Table 15.1), so one may suggest that the less soluble PDMS blocks self-aggregate into the core to minimize contact with the solvent and the soluble PAA chains form the diffuse corona of the micellar-like aggregations. As observed, the spheres are relatively homogenous in terms of stiffness (no contrast among the spheres on the stiffness image in Fig. 15.5). In addition, the adhesion image shows lower adhesion for bright spheres on the height image (dark ones on the adhesion image) and stronger adhesion for dark spheres on the height image (bright ones on the adhesion image). The different adhesion may be caused by the different contact areas between the AFM tip and the surface, which is one of the major factors determining the adhesion strength [63].

After we have found out that PDMS-*b*-PAA copolymer in the THF/MeOH mixture (1:1) forms micellar-like structures, our interest was set to investigate the

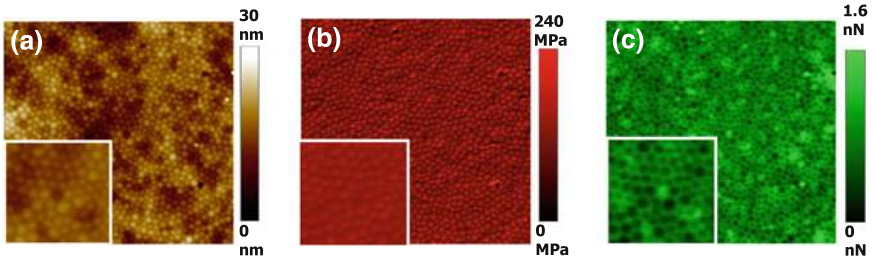

Fig. 15.5 PFT-AFM images (2 μm × 2 μm and a zoom 500 nm × 500 nm) of PDMS-*b*-PAA copolymer (M_n^{PDMS} = 10,000, M_n^{PAA} = 12,100) in an equal mixture of THF and MeOH (1:1) (0.1 g/mL). **a** Height; **b** stiffness and **c** adhesion

influence of the copolymer concentration on the size of the micelles. Copolymer solutions with different concentrations (20; 50 and 100 mg/mL) in a 1:1 ratio mixture of THF and MeOH were used. The images presented in Fig. 15.6 show the same spherical morphology for copolymer films prepared from three different concentrations. This observation leads us to the conclusion that the morphology is independent of the concentration. An increase in the aggregation size is observed (32 ± 3; 42 ± 3 and 50 ± 4 nm, at concentration 20; 50 and 100 mg/mL, respectively).

The fact that the micelle size depends on the concentration is likely related to the equilibrium between the aggregates and the isolated molecules in the solution. By increasing the concentration, the number of molecules in equilibrium to form the micelle (aggregation number) is favored in order to decrease the interface area between the solvent and the aggregating blocks [3]. This leads to an increase in the radius of the micelle core, which reflects on the size of the micelle.

As previously mentioned, the solvent has also a strong influence on micellar-like morphologies. Depending on the nature of the solvent, the self-assembly of block copolymers leads to formation of various morphologies. In this study, the influence of different solvents, THF (selective solvent for PDMS), MeOH (selective solvent for PAA) and also the mixture of both of them, on surface morphologies was investigated in detail.

The height image presented in Fig. 15.7a shows cylindrical objects (rod-like aggregates) for the PDMS-*b*-PAA copolymer in pure THF. In this case, it is expected that the PAA sequences assemble into the core while the PDMS blocks form the corona. The cylinders have an apparently uniform width of 56 ± 7 nm, but are rather polydisperse in length, lying in the 90–550 nm range. Most aggregates appear to be bent rather than straight cylinders. The results obtained with the (9:1) THF/MeOH mixture show the presence of both spherical and cylindrical micelles (Fig. 15.7b). This suggests that these two types of organizations have similar stabilities in the solvent mixture. With further addition of MeOH, moving to the (1:1) THF/MeOH mixture and then to pure MeOH (by increasing the content of MeOH to the (1:1) in THF/MeOH mixture and then moving to pure MeOH), a fully

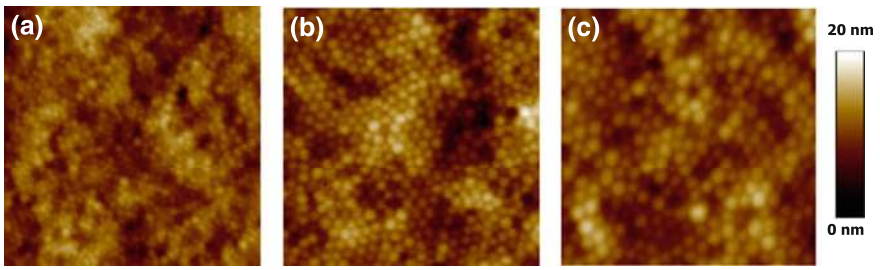

Fig. 15.6 Topography images (1 μm × 1 μm) of PDMS-*b*-PAA copolymer (M_n^{PDMS} = 10,000, M_n^{PAA} = 12,100) in THF/MeOH mixture (1:1) at different concentrations **a** 20 mg/mL; **b** 50 mg/mL and **c** 100 mg/mL

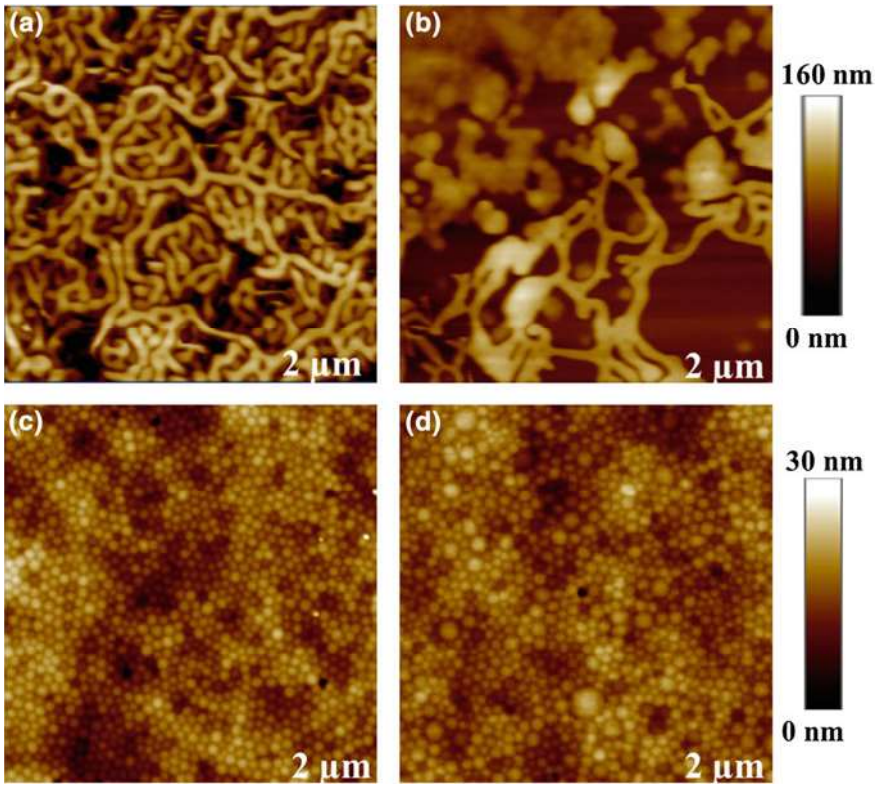

Fig. 15.7 PFT-AFM height images (2 µm × 2 µm) of PDMS-*b*-PAA copolymer in different solvents (100 mg/mL) **a** from pure THF, **b** from THF/MeOH mixture (9:1), **c** from THF/MeOH mixture (1:1), **d** from pure MeOH

spherical morphology is recovered and the size of the spheres is more homogenous (Fig. 15.7c, d, respectively).

The presence of different morphologies is probably related to polymer-solvent interactions (which are related to the difference between the solubility parameters of the polymer and the solvent). The formation of cylindrical aggregates may be caused by the particular orientation of the PAA cores in THF as its solubility parameter (δ_{PAA} = 24.6 $MPa^{1/2}$) is relatively close to the value of THF (δ_{THF} = 18.5 $MPa^{1/2}$) compared to the solubility parameter between PDMS (δ_{PDMS} = 14.6 $MPa^{1/2}$) and MeOH (δ_{MeOH} = 29.7 $MPa^{1/2}$).

With the addition of MeOH, the quality of the solvent for the PDMS blocks is expected to decrease gradually. This leads to the appearance of spherical micelles. Since MeOH is a selective solvent for the PAA blocks, it can swell the PAA cores and increases the mobility of the PAA chains. Therefore, the presence of MeOH leads to a reorganization of the system towards spherical objects. The sizes of the micelles generated in different solvents [THF, THF: MeOH (1:1) and MeOH] are

56 ± 7, 50 ± 4 and 57 ± 6, respectively. It is observed that the aggregates have a similar average size (considering the error bars). This is more likely due to the similar molecular weights of the PDMS and the PAA blocks (M_n^{PDMS} = 10,000, M_n^{PAA} = 12,100). In the case of the 1:1 THF/MeOH mixture, the micelle size seems to be more homogenous, probably as a result of a better solvation of the PAA chains. The solubility parameter of PAA (δ_{PAA} = 24.6 $MPa^{1/2}$) is indeed very similar to that of the THF/MeOH mixture ($\delta_{mixture}$ = 24.9 $MPa^{1/2}$). It means that these micelles also have considerable stability in the THF/MeOH mixture [64].

15.3 Incorporation of Block Copolymer into Silicone Coatings for Adhesive Applications

15.3.1 Coating Preparation

In this study, the modification of silicone coatings is achieved by incorporating amphiphilic block copolymers containing a PDMS segment which provides a good miscibility with the PDMS matrix and a segment of poly(acrylic acid) or poly ((2-dimethylamino) ethyl methacrylate) (PDMAEMA), or a modified-PDMAEMA segment [with quaternary amine (PDMATMA-I^-) or zwitterionic functions (PDMAEMA-SO_3^-)]. These second blocks bearing different functional groups will allow enhancing the surface wettability and also modifying the surface chemistry and adhesion after immersion in water, due to their hydrophilic character. As the PDMS-*b*-PDMAEMA-SO_3^- is not soluble in any solvent, dry condensation-curing is found to be a suitable technique to incorporate all copolymers in the silicone matrix.

In order to prepare these coatings, room temperature vulcanizing (RTV) silicone was purchased from ABCR, Germany. It consists of two parts: namely A and B, which have to be mixed together in a 10:1 weight ratio in order to obtain cross-linked materials. Part A initially contains a polymer base (silanol-terminated PDMS) and a crosslinking agent [poly (diethoxysiloxane)]. Part B contains a catalyst [DBTL (dibutyl tin dilaurate)] and trimethylsiloxy-terminated PDMS (PDMS-CH_3) was used to dilute the catalyst. A filler [silicon dioxide (silica), hexamethylsilazane surface-treated, ABCR Germany] was further added in order to improve the mechanical stability of the cured silicone.

The block copolymer-filled coatings were prepared as follows: first PDMS-OH and 2 wt% silica were mixed with a mechanical stirrer for 30 min. Then the block copolymer (5, 10, or 20 wt% for PDMS-*b*-PDMAEMA and 10 wt% for PDMS-*b*-PDMAEMA-SO_3^-, 10 wt% PDMS-*b*-PDMATMA-I^-, 10 wt% PDMS-*b*-PAA) in powder form was roll-milled within part A of the condensation-curing silicone. A three-roll milling machine (Exakt 80E, Exakt Advanced Technologies GmbH, Germany) set at room temperature, counter-rotation mode at 150 rpm, gap between the back and middle rolls 15 μm and between the middle and the front rolls 5 μm

was used. The roll-milling process was repeated three times. The obtained mixture was degassed in a vacuum oven, followed by addition of the crosslinker under stirring (silanol-terminated PDMS/crosslinker = 91/9 mass ratio). Then part B (PDMS-CH_3 and the catalyst—DBTL, 1 wt%) (10:1 mass ratio) was added and the mixture stirred at 500 rpm for 1 min. In this case, DBTL is a typical catalyst for condensation curing. It plays an important role in the crosslinking reaction between silanol-terminated PDMS and poly (diethoxysiloxane) (as shown in Fig. 15.8).

Finally, each mixture was spread on glass substrates (microscopy glass slides) by means of the Doctor-Blade method, which resulted in a coating thickness of about 300 μm. The glass slides (size 25 × 75 × 1 mm, VWR) were treated with a silane coupling agent (Primer OS1200, Dow Corning, Belgium) prior to deposition of the silicone coatings.

15.3.2 Contact Angle Measurements

Sessile drop water contact angle measurements on coatings before and after immersion in water were carried out with a Kruss DSA 10 apparatus. The hydrophobic/hydrophilic character of the PDMS layer was evaluated by measuring the static contact angle between the surface of the coating and demineralized water drops (ca. 30 μL). Advancing and receding contact angles were measured by increasing by 20 μL (growing phase) and then decreasing by 30 μL (contracting phase) the drop volume. A waiting period of 20 s, called the relaxing phase, was applied between the growing phase and the contracting phase. The data presented are the average of a minimum of five measurements on more than three different samples. All measurements were performed in ambient air at room temperature.

It is well known that adhesion is strongly dependent on the surface properties, such as wettability. In order to elucidate this point, the changes in the surface

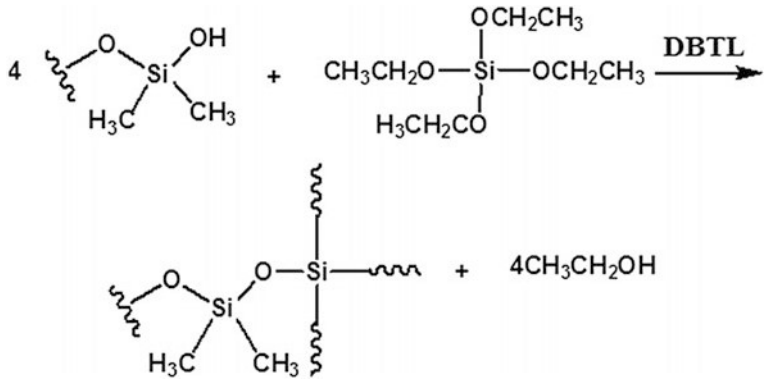

Fig. 15.8 Crosslinking reaction between silanol-terminated PDMS and poly (diethoxysiloxane)

wettability of PDMS upon addition of the copolymers were investigated in air by static contact angle (CA) and surface tension (γ_s) measurements. As underwater adhesion is aimed, measurements were performed before and after immersion in water for predetermined period(s). As is clear from the static contact angle measurements in air and before immersion in water, all the coatings exhibit a hydrophobic behavior, with contact angles exceeding 100° (Fig. 15.9). It means that all coatings exhibit hydrophobic behaviour before immersion in water; the presence of the copolymers does not seem to influence the coating wettability. Then, a gradual decrease of contact angle values was observed after immersing for 1, 3 and 4 weeks (as shown in Fig. 15.9).

According to the literature [48], after immersion in water the CA value measured for unfilled hydrosilylation-curing PDMS coatings dropped from 109° to 96°, showing some decrease in the surface hydrophobicity. This is reported to be a consequence of a reversible reorganization of the siloxane backbone and the methyl groups at the coating surface. The reversibility of the process for unfilled PDMS

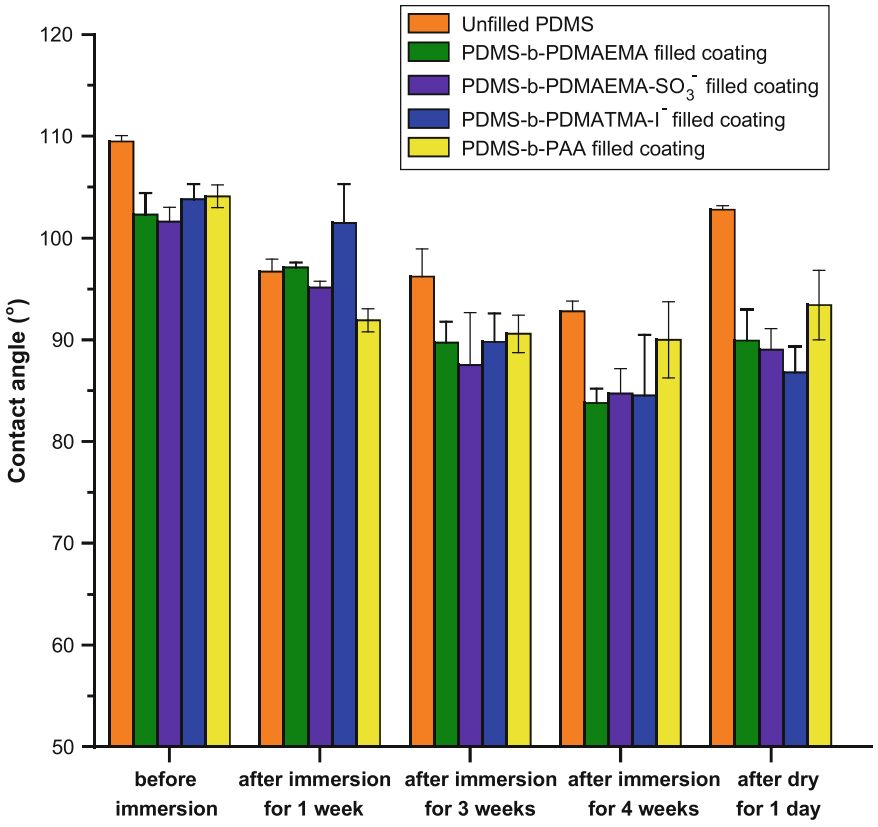

Fig. 15.9 Contact angles of PDMS and copolymer/PDMS coatings before and after immersion in water for different time

was confirmed by CA after drying at 80 °C for 24 h under reduced pressure (Fig. 15.9). Even if the exact nature of the process is not fully understood yet, it is supposed to be due to changes in the initial packing arrangement of the polymer chains, leading to surface reorganization and variations in terms of roughness and morphology [65]. In the case of the block copolymer-filled coatings, one observes a strong decrease in contact angle, from 102° to about 84° for PDMS-*b*-PDMAEMA; from 101° to about 85° for PDMS-*b*-PDMAEMA-SO_3^-, from 104° to 90° for PDMS-*b*-PAA filled coatings after 4 weeks of immersion. In fact, the average CA of copolymer-filled PDMS shifts to lower values (86°) in comparison with unfilled PDMS (96°), thus suggesting the occurrence of other processes besides the rearrangement of the polysiloxane chains. During the near-surface reorganization of the films, the amphiphilic block copolymer chains incorporated in PDMS coating could rearrange and move to locate at the outermost surface (as depicted in Fig. 15.10).

To confirm this hypothesis, coatings filled with 5, 10, 20 wt% of the PDMS-*b*-PDMAEMA block copolymer were prepared. The contact angle data for the coatings before and after immersion in water are presented in Fig. 15.11.

Before immersion, the wettability of the coating surface is not affected by the presence of the block copolymer, as the static contact angle remains in all cases close to 102°. Upon immersion in water, the contact angle of all coatings decreases with time, but it does much faster for 20 wt%-filled coatings than for the 5 wt%-filled ones. After immersion for 4 weeks, the contact angles for 10 and 20 wt% are quite similar, indicating that the maximum level of surface modification has been reached. Moreover, the reversibility of the process seems to be lost (Fig. 15.9): the CA of the copolymer/PDMS coatings insignificantly changed after drying (80 °C, 24 h, reduced pressure), thus confirming the presence of block copolymers on the coating surface.

These results are further confirmed by surface tension measurements. The surface tension of the coatings was evaluated also by measuring the contact angles with polar (water) and non-polar (diiodomethane and n-hexadecane) liquids and calculated using the Owens-Wendt-Young equation:

$$\gamma_L(1+\cos\theta)/2{\gamma_L}^{d1/2} = {\gamma_S}^{d1/2} + {\gamma_S}^{p1/2}\left({\gamma_L}^{p}/{\gamma_L}^{d}\right)^{1/2}$$

where θ is the contact angle, γ^d and γ^p refer to surface tension arising from dispersion forces and polar interactions, respectively, and the subscripts L and S refer to the contact-angle test liquids and solid, respectively. Table 15.2 shows the surface tension (γ_s) values of all coatings at 20 °C.

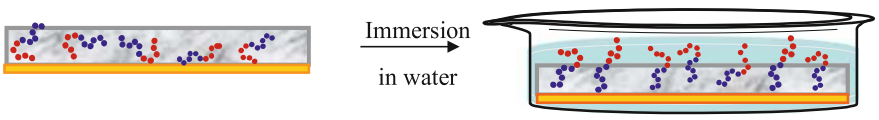

Fig. 15.10 Schematic representation of the reorganization of hydrophilic (*red chains*) and hydrophobic (*blue chains*) segments upon contact with water

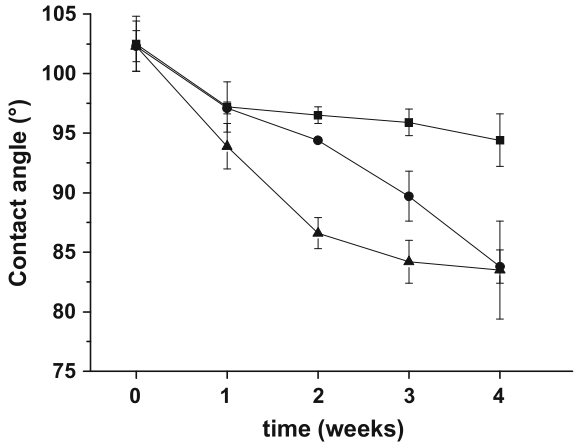

Fig. 15.11 Evolution of the contact angle (mean ± SD, n ≥ 5) of coatings filled with different amounts of PDMS-*b*-PDMAEMA copolymer (*filled square* 5 wt%; *filled circle* 10 wt%; *filled triangle* 20 wt%) with water-immersion time

Table 15.2 Surface tension (γ_s, mN m^{-1}) measurements of the condensation-cured silicone coatings

Samples	Surface tension (γ_s, mN m^{-1})		
	Before	After immersion	
		1 week	4 weeks
Unfilled PDMS	23.2	24.0	24.9
PDMS-*b*-PDMAEMA	23.2	25.8	28.1
PDMS-*b*-PDMAEMA-SO_3^-	23.8	26.5	29.8
PDMS-*b*-PDMAEMA-I^-	22.9	23.8	29.8
PDMS-*b*-PAA	23.4	23.8	26.3

Before immersion in water, the unfilled and copolymer-filled PDMS coatings exhibited relatively similar surface tension values of about 23 mN m^{-1}. Immersion leads to an increase in γ_s from 23.2 to 24.9 mN m^{-1} for unfilled PDMS. In the case of the copolymer-filled coatings, one observes a strong increase in the surface tension after immersion for 4 weeks, especially for PDMS-*b*-PDMAEMA; PDMS-*b*-PDMAEMA-SO_3^- and PDMS-*b*-PMAETMA-I^- for which γ_s rises from 23.2 to 28.1; from 23.8 to 29.8 and from 22.9 to 29.8 mN m^{-1}, respectively. Based on these results, one can imagine that the surface restructuring of PDMS chains allows penetration of water molecules in the near-surface layer. As a consequence, water molecules provoke conformational changes in the PDMS-*b*-PDMAEMA (PDMAEMA-SO_3^-) aggregates (see Surface Morphology section), bringing PDMAEMA (PDMAEMA-SO_3^-) segments to the surface. Thus, nitrogen and/or sulfur atoms should be present at the surface of the copolymer-filled PDMS coatings after immersion in water. This observation is confirmed using XPS analysis.

15.3.3 X-ray Photoelectron Spectroscopy Measurements

The surface composition of block copolymer-filled coatings was analyzed with X-ray Photoelectron Spectroscopy, using a VG ESCALAB 220iXL spectrometer. The XPS data were collected using monochromatic AlKα radiation at 1486.6 eV. Photoelectrons were collected from a 1 mm^2 sample area at take-off angle of 90°, giving an estimated probe depth of about 10 nm. For each sample, a survey spectrum was recorded with a 100 eV pass energy and 240 W of electron beam power, followed by high-resolution spectra for the C1s, O1s, Si2p and N1s peaks with a 31 eV pass energy. Atomic compositions were derived from peak areas using photoionization cross-sections calculated by Scofield, corrected for the dependence of the escape depth on the kinetic energy of the electrons and corrected for the analyzer transmission function of the spectrometer.

As immersed in water, all the coatings tend to be more hydrophilic. The molecular reorganization of PDMS and block copolymers upon contact with water gives the opportunity for the hydrophilic blocks to be exposed at the coating surface. In order to obtain information about the chemical composition of the pristine and the water-treated PDMS and copolymer-filled PDMS surfaces, XPS experiments were carried out on two coatings filled with PDMS-*b*-PDMAEMA and PDMS-*b*-PDMAEMA-SO_3^- copolymers. The results from the survey spectra of both coatings before immersion demonstrate the presence of three elements: silicon, oxygen and carbon typical of pristine PDMS, with peaks at 148, 102, 285, and 533 eV assigned to the Si_{2s}, Si_{2p}, C_{1s} and O_{1s}, respectively (Fig. 15.12a, c). After immersion in water, a new peak assigned to the N_{1s} level of PDMS-*b*-PDMAEMA appears in the spectrum (Fig. 15.12b, d).

The XPS spectra in the C_{1s} region (Fig. 15.13) were chosen to explain the copolymer-filled PDMS surface composition changes after immersion. As expected, only one peak at 284.4 eV, corresponding to the methyl groups of PDMS, is present for both coatings before immersion (Fig. 15.13a, c). After immersion in water for 4 weeks, the PDMS-*b*-PDMAEMA-filled coating shows a complex C_{1s} signal which can be curve-fitted into five components using the Voigt function (Fig. 15.13b). The component at 284.4 eV corresponds to the methyl groups of the PDMS backbone and the other four components, with binding energies between 284.9 and 288.8 eV, are typical of the PDMAEMA block. The component at 284.9 corresponds to –C–C/H groups; the contribution at 288.8 eV is due to COO groups, and the binding energy at 286.4 eV corresponds to the C–N and C–O-groups, which cannot be resolved [46]. The fourth component at 285.4 eV is characteristic of carbon atoms adjacent to the carbonyl group of the ester moiety (*C–(C=O)–O).

The C_{1s} fitting for the PDMS-*b*-PDMAEMA-SO_3^- filled systems reveals the presence of the peak at 284.4 eV corresponding to methyl groups of the PDMS block, along with five other distinct peaks for the PDMAEMA-SO_3^- block: 285.0 eV for C–C/H groups, at 285.7 eV for *C–COOH groups, at 286.6 eV for C–N groups, 287.7 eV for (C=O)–O–C* groups, at 288.8 eV for *CO (O) groups. The presence of $N^+(CH_2)_3SO_3^-$ groups is confirmed by peaks at 403.4 eV for

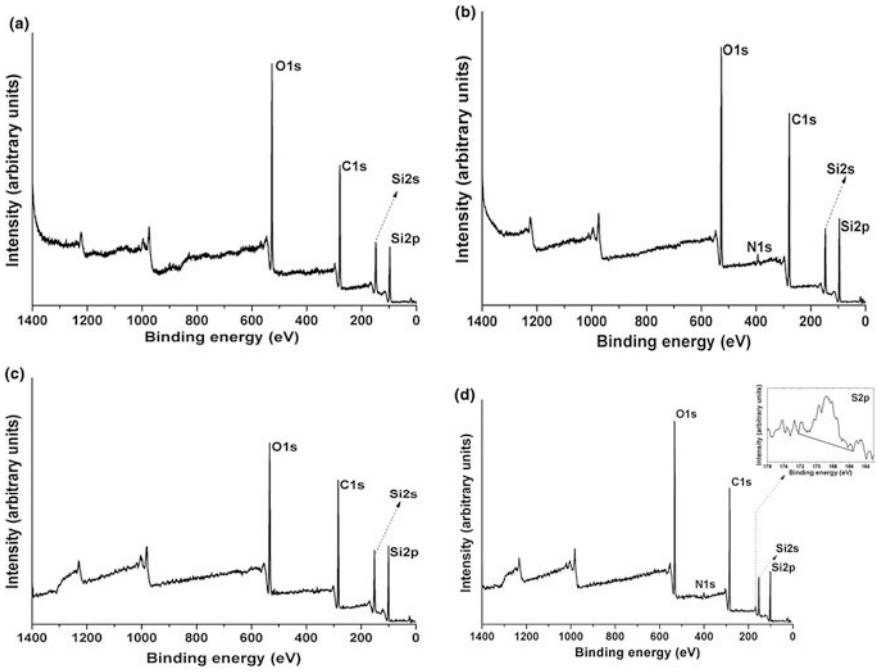

Fig. 15.12 XPS Survey spectra of 10 wt% PDMS-*b*-PDMAEMA filled silicone coatings **a** before; **b** after immersion and of 10 wt% PDMS-*b*-PDMAEMA-SO_3^- filled silicone coatings **c** before; **d** after immersion

quaternized nitrogen and at 168.0 eV for the sulfur atoms (Fig. 15.12d). The XPS results thus indicate that the PDMAEMA and PDMAEMA-SO_3^- blocks originally located underneath the surface of the coatings move to the surface upon prolonged contact with water. Moreover, considering that the repeating unit in PDMS polymer is Si $(CH_3)_2O$ and that of PDMAEMA is $C_8H_{15}O_2N$, one can assess the density of PDMAEMA after immersion in water by considering the Si/N atomic ratio after immersion: Si = 95.26% and N = 4.74%. Thus, for 10 wt% copolymer-filled PDMS coatings the PDMAEMA moieties occupy 4.74% of the surface of the sample (the thickness probed by the VG Escalab 220iXL spectrometer is estimated to be 10 nm).

15.3.4 Atomic Force Microscopy (AFM) Measurements in Air

AFM measurements were performed on the thin films using a Dimension Icon (Bruker Nano Inc., Santa Barbara, CA) and a Multimode 8 (driven by a

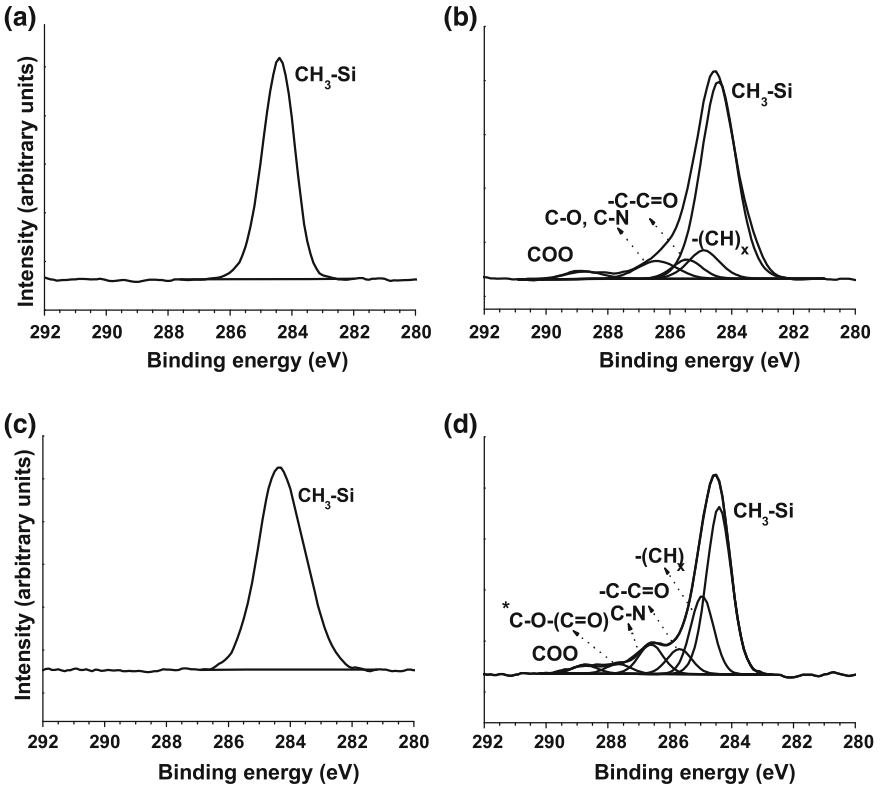

Fig. 15.13 XPS C1s spectra of PDMS-b-PDMAEMA-filled silicone coatings **a** before and **b** after immersion; and of PDMS-*b*-PDMAEMA-SO_3^- filled silicone coatings **c** before and **d** after immersion

Nanoscope V control unit) in air or dried after immersion in ultrapure MilliQ water, in ambient conditions. Two different types of samples (before and after immersion in water) were studied. The immersed coatings were dried with a nitrogen flow prior to measurement in air. For the samples analyzed in water, measurements with a specific cantilever holder were carried out in a fluid cell, in order to evaluate the variation in the surface morphology of the coatings upon immersion.

Imaging was performed in contact mode and Peak Force Tapping with a minimal applied force (250 pN for hydrophilic tips or 500 pN for hydrophobic tips). Unless otherwise specified, all force measurements were recorded with an approach and retraction speed of 1000 nm/s and a contact time lower than 50 ms. Adhesion maps (in force volume) were obtained by recording 32 × 32 force distance curves on areas of 5 μm × 5 μm, calculating the maximum adhesion peak and displaying the value as a gray pixel. PFT images were digitally recorded with a resolution of 512 pixels/line. The scan rate was kept at 0.5 Hz. For high ionic strength experiments,

0.1 M NaCl solutions were injected into the liquid cell 15 min prior to force measurements.

V-shaped silicon nitride probes ($k \sim 0.3$–0.4 N m^{-1}) with 115 μm narrow-legged cantilevers, CH_3-terminated and COOH-terminated tips were used on these samples. The surface roughness (R_a) over 5.0×5.0 μm^2 images was calculated using the Nanoscope Analysis software. For the measurements of the mechanical properties, the probe was calibrated on a stiff surface prior to the experiment, in order to quantify the tip-sample force. The spring constant was determined by the thermal tune technique.

The surface morphology of PDMS unfilled and filled coatings before immersion in water in air were obtained by AFM. It was found that, the unfilled PDMS films are homogenous and smooth (as illustrated in Fig. 15.14a), with a small roughness ($R_a \sim 1$ nm). The values obtained for the block copolymer filled samples show increasing in the roughness: $R_a \sim 14$ nm for the PDMS-*b*-PDMAEMA filled coating, $R_a \sim 3$ nm for the PDMS-*b*-PDMAEMA-SO_3^- filled coating and $R_a \sim 6$ nm for the PDMS-*b*-PAA filled coating. This increase is a result of the presence of rough round-shaped objects, which we call aggregates, on the coating surface. In the case of PDMS-*b*-PDMAEMA filled coatings (Fig. 15.14b), we observe very large aggregates compared with the coatings filled with PDMS-*b*-PDMAEMA-SO_3^- and PDMS-*b*-PDMATMA-I^- as well as PDMS-*b*-PAA (Fig. 15.14c–e, respectively). This may be related with our observation that PDMS-*b*-PDMAEMA has some synergetic effect onto the catalyst, making the crosslinking process faster (as a result, the curing time is shorter compared to coatings filled with the other copolymers). We thus propose that the aggregates shown on the AFM images are regions of the coating where the PDMS crosslinking has proceeded to a larger extent because of the presence of the copolymer below the surface, giving rise locally to a different morphology.

The formation of those aggregates is demonstrated more clearly by adding different amounts of the PDMS-*b*-PDMAEMA copolymer (5, 10, 20 wt%) in coatings.

As illustrated in Fig. 15.15, the increase of the copolymer amount (from 5 to 20 wt%) leads to an increase in the number of aggregates. The proportion of aggregates can be estimated by directly measuring the number and the size of the objects present on the images. These proportions are 11, 30 and 47% for the coating containing 5, 10, and 20 wt% copolymer, respectively. This observation suggests that the aggregates are: (i) related to the presence of copolymer; (ii) not the copolymer itself (since the XPS data show the absence of copolymer on the surface). This leads to our hypothesis that the aggregates are regions with a higher density of crosslinking because of a local increase in the amount of copolymer below the surface. The synergistic effect [66] of the PDMS-*b*-PDMAEMA copolymer on the crosslinking reaction is probably due to the amino groups of PDMAEMA, which can improve the activity of the DBTL catalyst during the crosslinking process. This would explain that the formation of aggregates is less prominent when the polymer is protonated (PDMS-*b*-PDMAEMA-SO_3^-) or

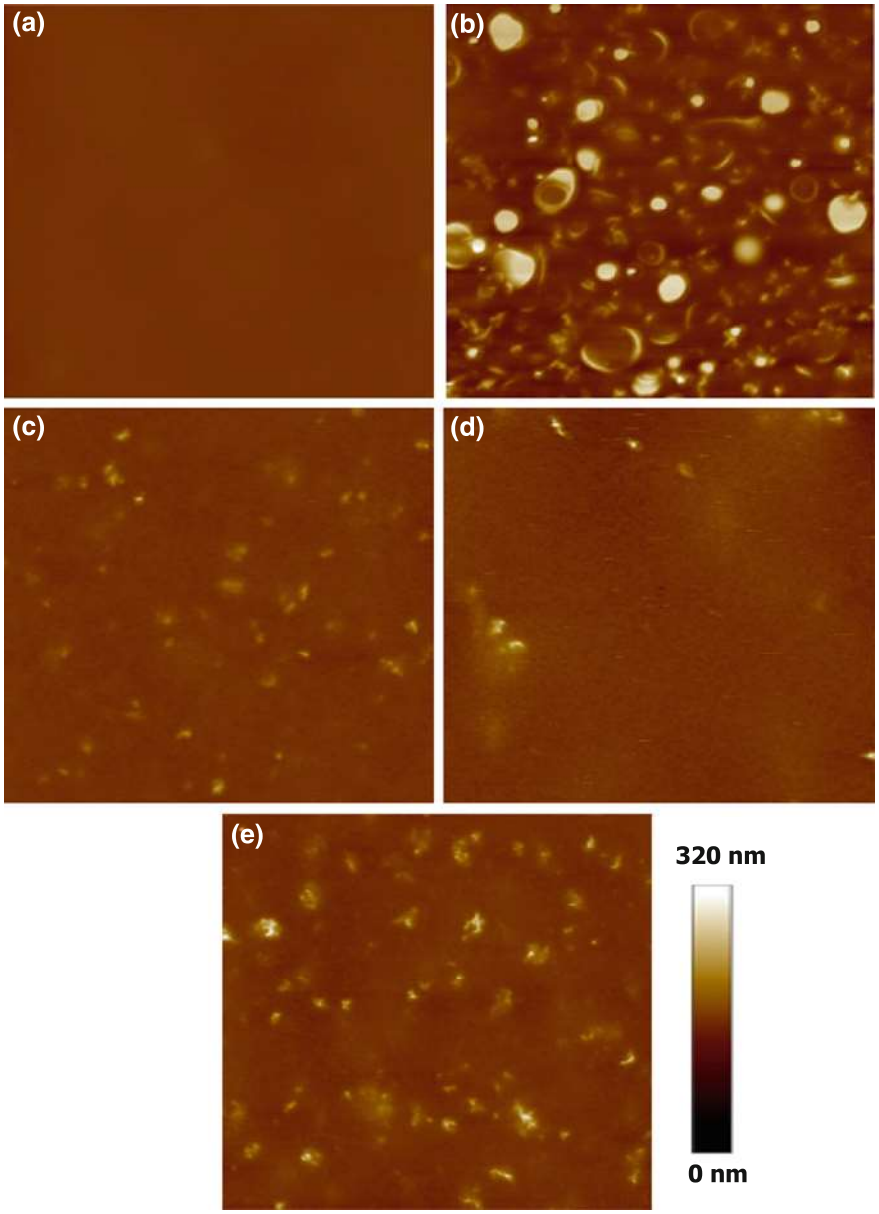

Fig. 15.14 Topography images (5 μm × 5 μm) of different coatings: **a** PDMS unfilled; **b** filled with 10 wt% PDMS-*b*-PDMAEMA; **c** filled with 10 wt% PDMS-*b*-PDMAEMA-SO_3^-; **d** filled with 10 wt% PDMS-*b*-PDMATMA-I^-; **e** filled with 10 wt% PDMS-*b*-PAA copolymers

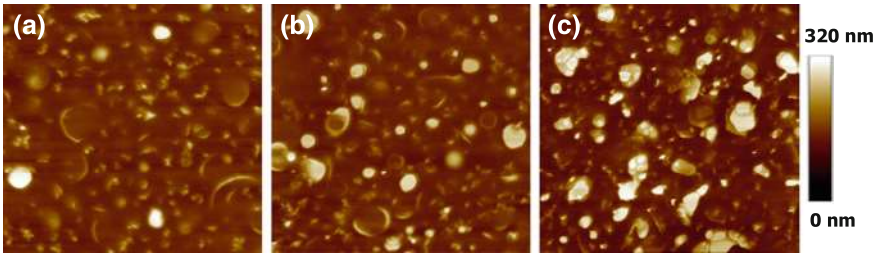

Fig. 15.15 PFT-AFM height images (5 μm × 5 μm) of PDMS filled with different amounts of PDMS-*b*-PDMAEMA copolymer before immersion in water **a** 5 wt%; **b** 10 wt% and **c** 20 wt%

quaternized (PDMS-*b*-PMAETMA-I^-), i.e., when the amino groups have been turned into ammonium groups.

Following the initial experiments, some extra measurements were carried out on dry samples immediately after their removal from water.

The unfilled PDMS coating after immersion shows a slight change in the surface topography (with the appearance of some higher spots on the surface, as shown in Fig. 15.16d) and an increase of the roughness (from $R_a \sim 1$ to 3 nm). It may be the result of the surface reorganization due to the flexibility of PDMS chains and/or some penetration of water in the silicone coatings. An increase in roughness is also observed for the PDMS-*b*-PDMAEMA filled coatings (from $R_a \sim 14$ to 20 nm) and the PDMS-*b*-PDMAEMA-SO_3^- filled coatings (from $R_a \sim 3$ to 6 nm). Interestingly, the morphology is clearly modified for those two materials: in the case of the PDMS-*b*-PDMAEMA filled coatings, the microdomains with "round" like shapes observed before immersion (Fig. 15.16b) turn to microdomains with irregular contours (Fig. 15.16e). In the PDMS-*b*-PDMAEMA-SO_3^- filled coatings, the surface after immersion shows elongated or star-like objects (Fig. 15.16f). This may be the result of the swelling of the aggregates during the immersion step, followed by drying prior to the AFM measurements (compare with the AFM data recorded in water below).

15.3.5 Atomic Force Microscopy (AFM) Measurements in Water

Quantitative measurements of the adhesion force are appropriately performed in liquid by using PFT technique, in order to eliminate the effect of the thin adsorbed water layer present on the surfaces in air. The results obtained for 10% PDMS-*b*-PDMAEMA filled coatings are shown in Fig. 15.17.

The aggregates are still present when the coating is immersed, but their shape appears to have changed, as seen in the height images (insets of Fig. 15.17a, b); the aggregates, which are rather dense in the dry coating, turn to a "flower-like" shape

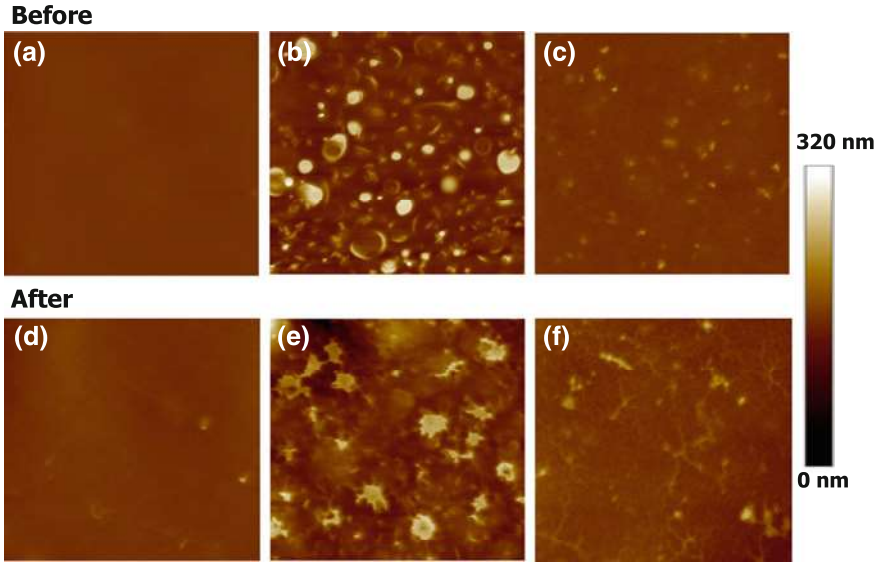

Fig. 15.16 Height images (5 µm × 5 µm) of **a**, **d** unfilled PDMS, **b**, **e** filled with 10 wt% PDMS-*b*-PDMAEMA and **c**, **f** filled with 10 wt% PDMS-*b*-PDMAEMA-SO_3^- before and after immersion in water, respectively

after immersion in water. This is believed to be the result of the reorganization of copolymer chains with the migration of hydrophilic chains on top of the surface (as indicated by the increase in wettability and the appearance of peaks typical for the hydrophilic blocks in the XPS spectra). This migration may be somewhat hampered in the areas where the PDMS is more densely cross-linked, compared to other parts of the surface, which may lead to the open aggregates on the coating surface after immersion.

Regarding the mechanical properties, it is interesting to note that, when immersed in water, these aggregates are softer than the matrix (they appear darker in the stiffness image), owing to water absorption by hydrophilic chains at the surface of the coatings. In addition, one observes that the highly cross-linked aggregates are less adhesive than the surface of the matrix (as shown in Fig. 15.17e, f). The corresponding adhesion histograms (Fig. 15.18) demonstrate the modification of adhesive distribution on the surface after immersion.

Figure 15.18a shows a narrow distribution of adhesion values (most values are found around 1800 pN) for the initial coating, while a broader distribution is obtained in the case of the immersed coating (Fig. 15.18b): the adhesion values lie in the 100–2500 pN range. The higher peak in Fig. 15.18a corresponds to the adhesion value of the PDMS matrix while the contribution around 500 pN is due to the aggregates, which are less adhesive. The adhesion shows a tendency to decrease after immersion, as can be seen in Fig. 15.18b. The adhesion values around 500 pN are still attributed to the aggregates. Adhesion values around 1800 pN become less

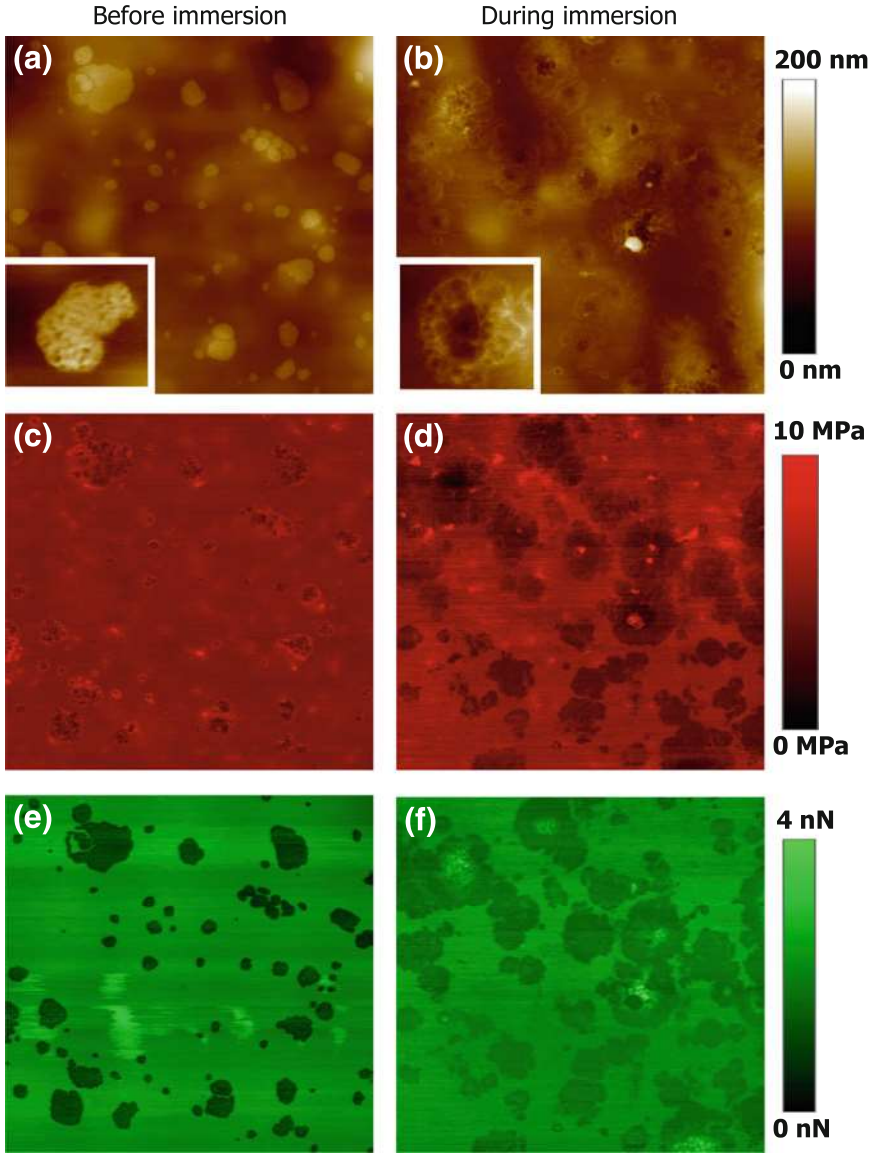

Fig. 15.17 PFT-AFM images obtained in water **a**, **b** height; **c**, **d** stiffness and **e**, **f** adhesion of 10 wt% PDMS-*b*-PDMAEMA filled coatings before and during immersion in water, respectively

frequent whereas an increase in frequency of the adhesion force ranging from 1000 to 1500 pN is observed (Fig. 15.18b). As shown above by the contact angle measurements, the coating surface after immersion becomes more hydrophilic, due to the reorganisation of copolymer chains. The modification of the adhesion can be

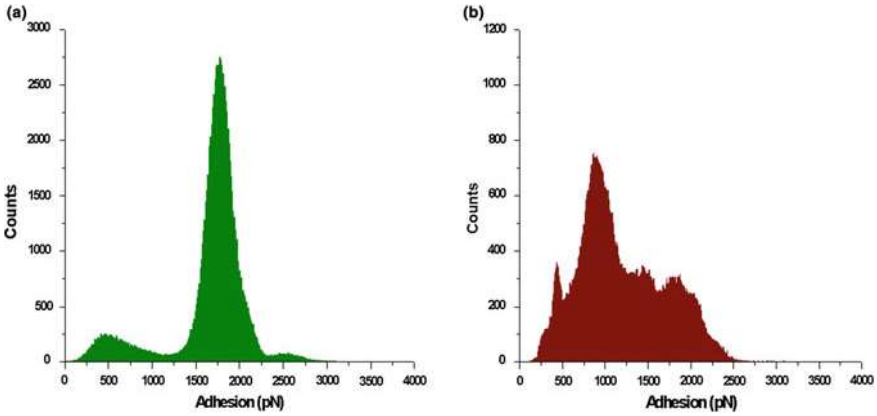

Fig. 15.18 Adhesion histograms of 10 wt% PDMS-*b*-PDMAEMA filled coatings obtained from AFM imaging in water: **a** initial coating (immersion time = 0); **b** immersed coating (immersion time = 4 weeks)

related to the different interactions between hydrophilic/hydrophobic surfaces and the silicon tip in aqueous solution. Based on the water structure rearrangement when an initially hydrophobic or hydrophilic surface comes into contact with water, Israelachvili et al. [67, 68] demonstrated that the orientation of the water molecules in the first layer next to hydrophobic or hydrophilic solid surfaces is quite different. They observed the existence of tangential alignment of the water molecules near hydrophobic surfaces, whereas normal alignment of the water molecules takes place at hydrophilic surfaces. The molecular reorganization of water on the hydrophobic substrate involves entropic effects due to the increase of hydrogen bond formation, which leads to a stronger attractive force with a hydrophilic probe surface, compared to hydrophilic substrates [69, 70]. In our case, the silicon tip is covered by a thin SiO_2 layer, which makes it hydrophilic in water. Hence, the interaction force between two hydrophilic surfaces is lower than that between one hydrophobic and one hydrophilic surface. We therefore believe that the broadening of the adhesion distribution of the immersed coatings reflects the reduction of hydrophobicity at the surface (as indicated by the decrease of contact angle after immersion), as well as the different adhesion forces between the hydrophilic/hydrophobic surfaces with the silicon tip in water. The difference of tip-surface interaction forces will then be clarified by employing AFM functionalized tips.

Figure 15.19 shows contact mode AFM topographic images recorded in milliQ water of 10 wt% PDMS-*b*-PDMAEMA copolymer-filled silicone coatings before and after immersion in water. It was found that the aggregates present on the coating surfaces before immersion (Fig. 15.18a) turn to a "flower-like" shape after immersion (Fig. 15.19b). This observation is in a good agreement with the results obtained by Peak Force Tapping (Fig. 15.16a, b). It means that contact mode AFM with minimal applied force does not damage the coating surface. Immersion in water led to a rearrangement of the coating structure, with the transfer of the

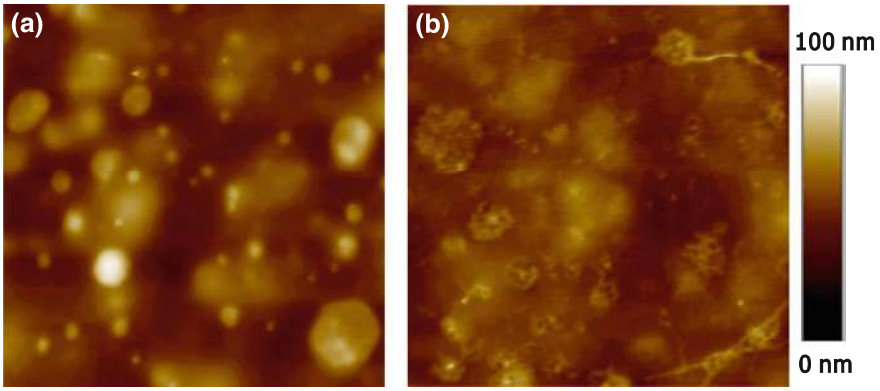

Fig. 15.19 Contact mode AFM height images (5 μm × 5 μm) of 10 wt% PDMS-*b*-PDMAEMA-filled silicone coatings **a** initial coating (immersion time: 0); **b** immersed coating (immersion time: 4 weeks)

hydrophilic blocks to the surface. This reorganization resulted in changes of the surface morphology and adhesive properties of the coatings.

As described above, Chemical Force Microscopy can also provide the adhesion properties of silicone-based coatings measured by using functionalized probe tips. Here we first used adhesion force mapping with hydrophobic tips (CH_3-terminated alkanethiols) to probe the local hydrophobic properties of the copolymer-filled coating surfaces before and after prolonged immersion in water.

Figure 15.20a, b shows the adhesion force maps, adhesion force histograms and representative force curves, recorded in milliQ water with hydrophobic tips on the 10 wt% PDMS-*b*-PDMAEMA copolymer-filled silicone coating before prolonged immersion in water. Most force curves recorded across the surfaces showed large adhesion forces, with a mean magnitude of 5.5 ± 0.4 nN (n = 2048 force curves from two maps obtained using different tips and samples). Comparison with the data obtained on reference surfaces [69] revealed that the polymer surface had a marked hydrophobic character, equivalent to that of a self-assembled monolayer composed of 80% CH_3-terminated and 20% OH-terminated alkanethiols. In addition, adhesion maps showed homogeneous contrast, meaning the surface is entirely hydrophobic. Taken together, these observations indicate that the surface of the initial copolymer-filled coating is homogeneously covered with hydrophobic PDMS.

The observations for immersed coatings show lower adhesion forces (as seen in Fig. 15.20c, d), indicating that those coatings are more hydrophilic after prolonged immersion in water. Interestingly, the adhesion maps were heterogeneous, hydrophilic nanoscale patches (0.9 ± 0.4 nN) being observed in a more hydrophobic matrix (3.1 ± 0.3 nN). As these patches correlate with the heterogeneous surface morphology (Fig. 15.19c), we believe this heterogeneous hydrophobic contrast reflects the coexistence of the hydrophilic PDMAEMA and the hydrophobic PDMS

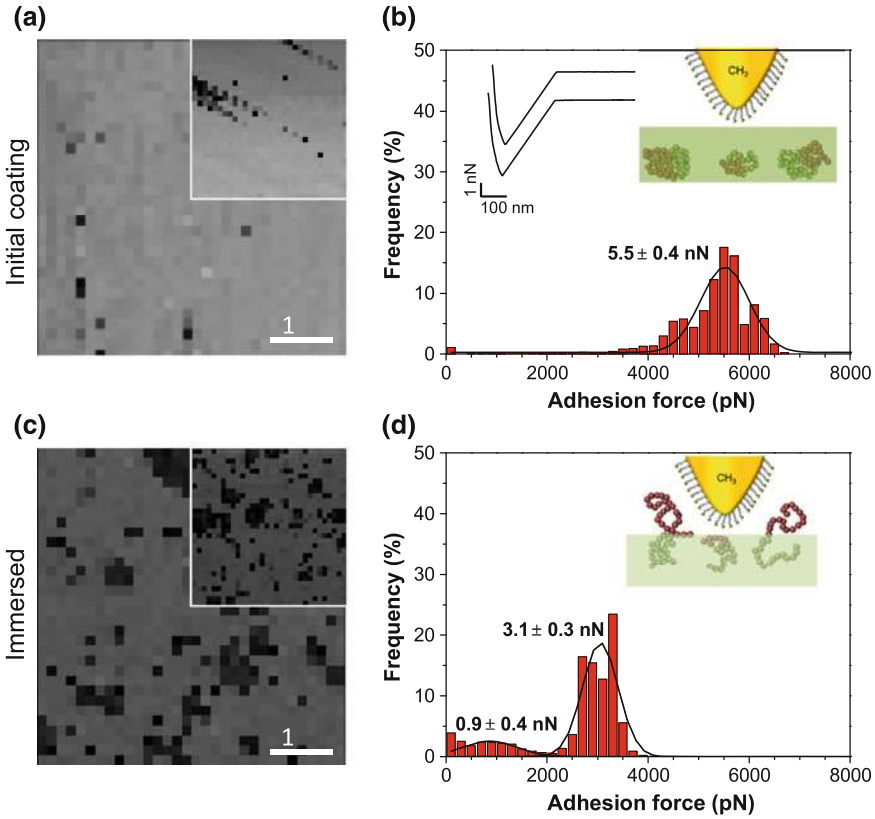

Fig. 15.20 Adhesion force maps (**a**, **c**) (5 μm × 5 μm) and **b**, **d** corresponding adhesion force histograms recorded in milliQ water with CH_3-terminated tips on **a**, **b** initial samples and **c**, **d** immersed samples

chains on top of the immersed-coating surface. That the surface hydrophobicity of silicone coatings decreased upon contact with water is consistent with earlier contact angle measurements (as shown in Fig. 15.9) [70–72]. Static contact angle measurements showed that both unfilled PDMS and PDMS-*b*-PDMAEMA-filled PDMS coatings exhibit a hydrophobic behaviour, with contact angles exceeding 100° before immersion in water. After 4 weeks of immersion, the contact angle value measured for unfilled PDMS coatings decreased to 96°, an effect believed to be a consequence of a reorganization of the siloxane backbone and the methyl groups at the coating surface. Interestingly, for the block copolymer-filled coatings, the average value of the contact angle shifted to even lower values (down to 84°), thus suggesting the occurrence of other processes, besides the rearrangement of the polysiloxane chains. Based on these results, one can imagine that the surface restructuring of flexible PDMS chains allows penetration of water molecules into the near-surface layer. As a consequence, water molecules would provoke

conformational changes in the PDMS-*b*-PDMAEMA-formed aggregates, bringing PDMAEMA segments to the surface. Thus, nitrogen atoms should be present at the surface of the PDMS-*b*-PDMAEMA-filled coatings after immersion in water, which was indeed confirmed by XPS analyses (Figs. 15.12 and 15.13) [72]. Upon immersion in water, interactions between methyl groups and water molecules are expected to induce molecular reorganisation of the polymer, tilting the polar oxygen groups toward the PDMS-water interface to minimise the surface energy [47].

These results also confirmed that the interaction force between two hydrophobic surfaces is larger than that between hydrophobic and hydrophilic surfaces as a result of the existence of hydrophobic attraction between two hydrophobic surfaces in aqueous media [73, 74].

As the PDMAEMA blocks in PDMS-*b*-PDMAEMA chains carry positively chargeable amino groups, they could also present specific interactions with COOH-terminated alkanethiol tips. Different tip-surface interaction forces are investigated depending on environmental conditions (the pH and the ionic strength of aqueous media) and dynamic changes of polyelectrolyte desorption.

Figure 15.21a–c shows the adhesion force maps, adhesion force histograms and representative force curves recorded in milliQ water (pH ~ 6) with COOH-terminated tips on immersed coatings. Based on pK_a of COOH and NH_2 groups (pK_a^{COOH}: 4.8; pK_a^{NH}: 7.5), the $–NR_2$ groups (R=CH_3) of the PDMAEMA [$–CH_2–C(CH_3)(COOCH_2CH_2N(CH_3)_2)–$] can be protonated to form $–NHR_2^+$ while the COOH groups can be deprotonated to form COO^- in milliQ water. Electrostatic interactions are therefore present in this case.

It is observed that the adhesion maps are highly contrasted, a large fraction of the curves (59%) showing adhesion forces ranging from 100 to 1800 pN. The adhesive signatures exhibited two types of behaviors, that is, constant plateau forces with extended rupture lengths (14%) or single linear force peaks with short rupture length (45%). The initial force peaks are attributed to the rupture of cohesive electrostatic bonds between the charged tip and the sample surface, and the plateau forces to the stretching of individual copolymer chains [75, 76].

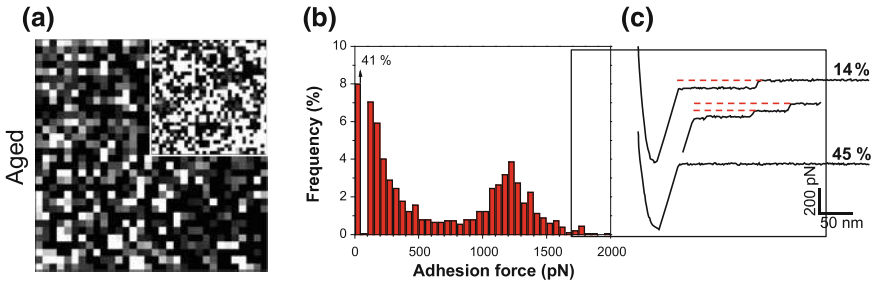

Fig. 15.21 **a** Adhesion force map (5 µm × 5 µm), **b** corresponding adhesion force histogram, and **c** representative force curves recorded using COO^--terminated tips on immersed sample in milliQ water

Plateau forces exhibit uniform rupture forces of 82 ± 7 pN magnitude, but variable rupture lengths (from 70 to 700 nm) due to the location of molecules at different points on the tip and/or on the sample surfaces [76]. These forces correspond to either continuous desorption (Fig. 15.22a, b) of individual polymer chains which detach, together with the retraction of cantilever to the rest position, or the progressive stretching (Fig. 15.22c, d) of single PDMAEMA chains from the tip surface [75–78]. In the latter case, during approach-retraction cycles, the polymer chains tend to bridge the tip and the substrate, and then desorb from the substrate. The first peak is characteristic of an attractive force that decreases rapidly and linearly with distance. After the jump-off-contact, the cantilever returns to the original position (zero deflection). The tip and sample seem to be detached, but some molecules are still bound by bonds which are stretched along the subsequent attractive surge until the force reaches a rupture value [76]. The interruption of 200 pN at a distance of 150 nm (green circle in Fig. 15.21d) indicates the detachment due to the rupture of the specific bonds between these molecules.

In addition, multiple plateaus are sometimes observed, reflecting detachment of multiples chain (Fig. 15.22b, e) [79, 80]. Note that adhesion maps did not show nanoscale domains and that the adhesion frequency (59%) was much larger than the fraction (10 wt%) of block copolymer introduced in the cross-linked PDMS matrix. This observation confirms that the copolymer preferentially locates at the coating surface.

To assess whether these polyelectrolyte interactions can be controlled by environmental conditions, we probed immersed copolymer-coatings at high ionic strength (in 0.1 M NaCl solution). Figure 15.23 shows the force data obtained using the same tips and samples as in Fig. 15.20 following injection of 0.1 M NaCl solutions.

As can be seen, the presence of salts led to a major decrease in the adhesion frequency from 59 to 16%, and the disappearance of most plateau forces, from 14 to 1%. The adhesion forces are also diminished down to less than 1200 pN with the most frequent values around 100 pN (84%). Since NaCl is an electrolyte, it is ionized into Na^+ and Cl^- ions in water. The $–NHR_2^+/COO^-$ interactions are therefore affected due to the formation of electrostatic interactions between COO^-/Na^+ and $–NHR_2^+/Cl^-$ ions. This leads to a strong decrease of the attractive interactions between the tip and the surface, explaining the decrease of the measured adhesion values.

In this systematic study, we also investigated the dynamics of polymer desorption by recording force curves at various pulling speeds and contact times.

As can be seen in Fig. 15.24a, b, plateau forces did not depend on the retraction speed, a behaviour clearly different from receptor-ligand unbinding forces [81] and protein unfolding forces [82]. This phenomenon, similar to that observed for amyloids [83] and polymer chains [79, 84], indicates that the measurements were made near thermodynamic equilibrium, thus the bonds involved in the desorption process dissociate and re-associate on a much faster timescale than the retraction speed of the tip. Figure 15.23c shows that increasing the pulling speed from 100 to 10,000 nm/s drastically decreased the plateau frequency, indicating that the occurrence of desorption events depends on the separation rate. To check whether

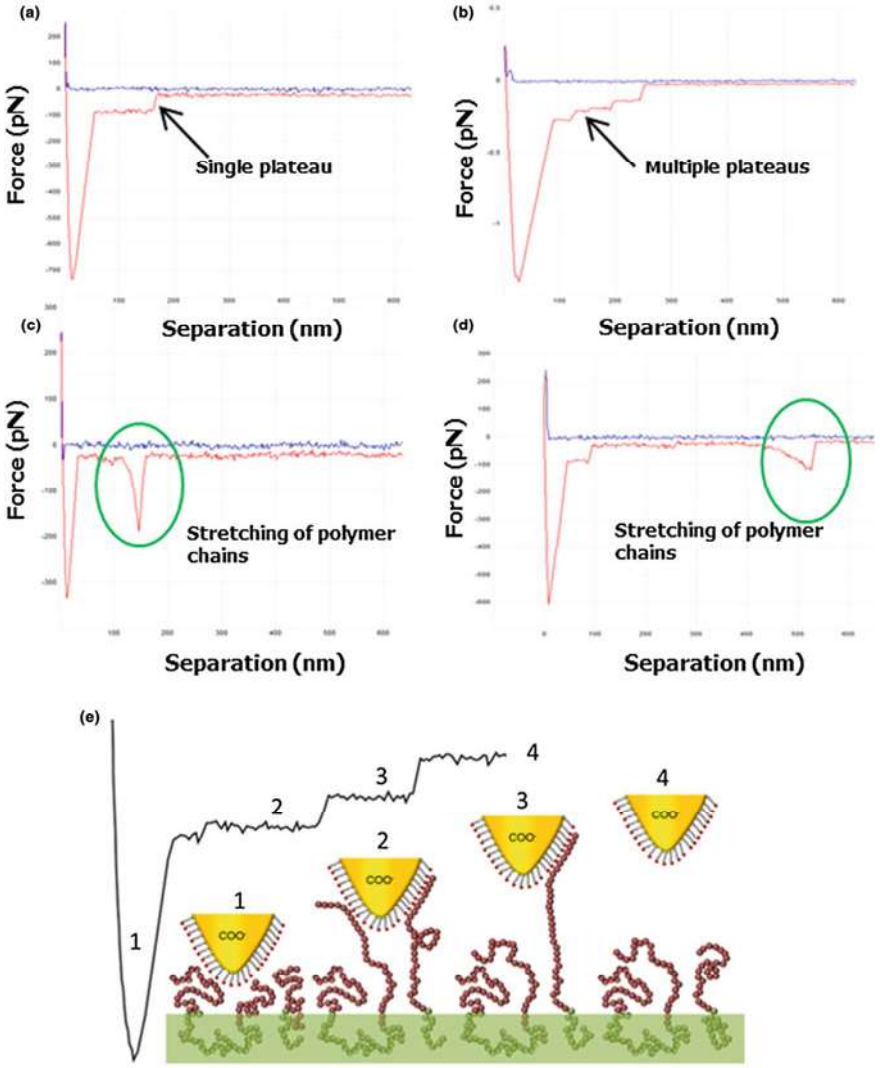

Fig. 15.22 **a–d**Representative force curves recorded for 10 wt% PDMS-*b*-PDMAEMA-filled silicone coatings after immersion in water: **a**, **b** plateau force curves represent continuous desorption of polymer chains from the tip surface **a** single plateau, **b** multiple plateaus; **c**, **d** force curves represent the progressive stretching of single polymer chain; **e** scheme representing detachment of multiples chains

this could be due to a time dependence in the desorption interaction, the contact time was varied while keeping the pulling rate constant (1000 nm/s). Under these conditions, no variation in plateau force frequency was observed (Fig. 15.24d), suggesting that the electrostatic interaction bridging the polymer to the tip is a fast process.

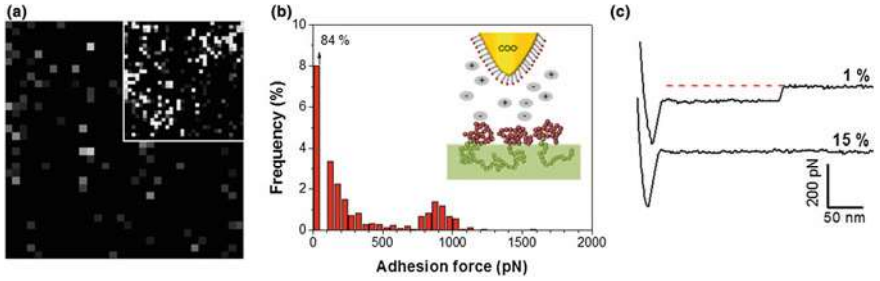

Fig. 15.23 **a** Adhesion force map (5 μm × 5 μm, *gray scale* 1000 pN), **b** corresponding adhesion force histogram, and **c** representative force curves recorded using COO^--terminated tips on immersed sample in 0.1 M NaCl solution

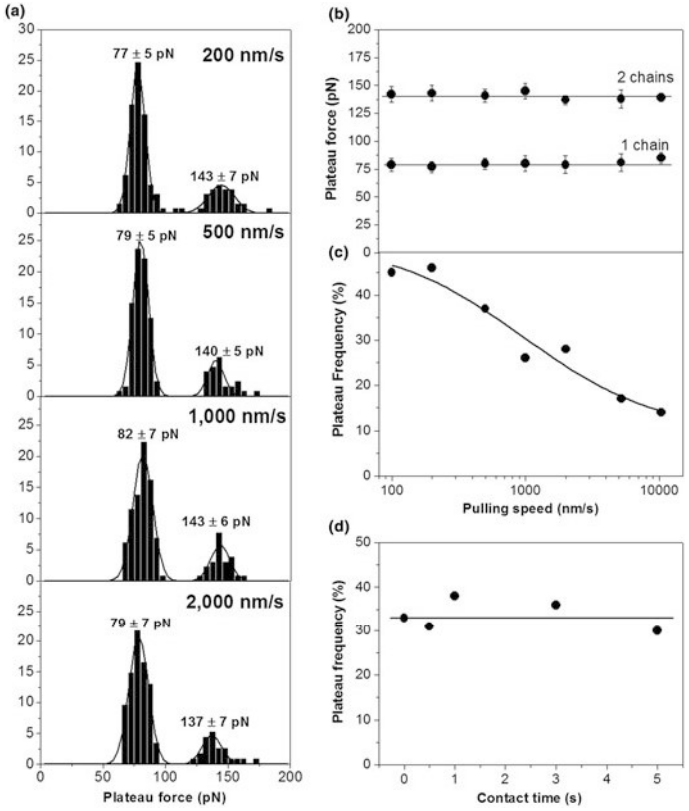

Fig. 15.24 **a** Histograms showing the distribution of plateau forces at different pulling speeds; **b**, **c** dependence of the mean plateau force (**b**) and force plateau frequency (**c**) on the pulling speed. **d** Dependence of the plateau force frequency on contact time measured at a constant pulling speed of 1000 nm/s

15.3.6 Bio-adhesion Testing

Finally, the bio-adhesion of the modified PDMS-based coatings were analyzed. Marine mussels are well known for their ability to adhere to a variety of surfaces by using a protein-based adhesive structure, the byssus. The byssus consists of a bundle of threads connected proximally to the base of the animal foot, within the shell, and terminating distally with a flattened plaque which mediates adhesion to the substrate [80]. The attachment process starts with the extension of the foot from the shell and contact with the surface. During this contact, the proteins stockpiled in the foot are secreted in a groove running along the length of the foot where they self-assemble. After a few seconds, the foot retracts, leaving a plaque adhering to the substratum with a complete thread which emerges from the groove as the foot is withdrawn [85]. This process is repeated several times and when the complete set of byssus threads is formed, the mussel is tethered to the substrate. Previous studies reported that the mussels can make a choice regarding the substrate to which the byssus is produced [85] and that, in general, they attach more rapidly to high energy surfaces than to lower energy surfaces [86].

In this work, bio-adhesion experiments with mussels have been performed on the different types of substrates—PDMS coatings unfilled and filled with block copolymers, before and after immersion in water. Common blue mussels, *Mytilus edulis*, were used, for which byssal plaque adhesion can be easily quantified in a controlled laboratory setting. For the experiments, individual animals were rubber-banded to microscope glass slides covered with the studied silicone coatings (Fig. 15.25a). After 2 or 3 days, production of byssal threads was recorded for each mussel and, when threads were present, traction tests were performed to measure the detachment force of their plaque.

The results reveal that the mussels usually do not produce byssal threads onto the unfilled PDMS coatings, neither before nor after immersion in water. Only one individual produced a few threads on one immersed coating but they were too small to be used for traction tests. As far as the studied block copolymer-filled coatings were concerned, the adhesion of mussels only took place on coatings which were first immersed in water for 4 weeks, i.e., when the copolymer is present at the surface (Fig. 15.25b). Indeed, 2 and 3 mussels attached to the PDMS-*b*-PDMAEMA filled coatings and the PDMS-*b*-PDMAEMA-SO_3^- filled coatings, respectively. On the other hand, mussels never produced byssal threads on the block copolymer-filled coatings that were not previously immersed. The detachment forces measured for the two copolymer-filled silicone coatings after 4 weeks immersion in water are presented in Fig. 15.25c, where the forces are averaged from the data measured for individual plaques. Both values are in the same range: 0.068 ± 0.018 N for the PDMS-*b*-PDMAEMA filled coatings and 0.079 ± 0.029 N for the PDMS-*b*-PDMAEMA-SO_3^- filled coatings.

This clearly highlights that both the immersion treatment and the presence of block copolymers play a significant role in the attachment of mussels to the coatings. When looking at the surface energy of the coatings, the mussels attach to the

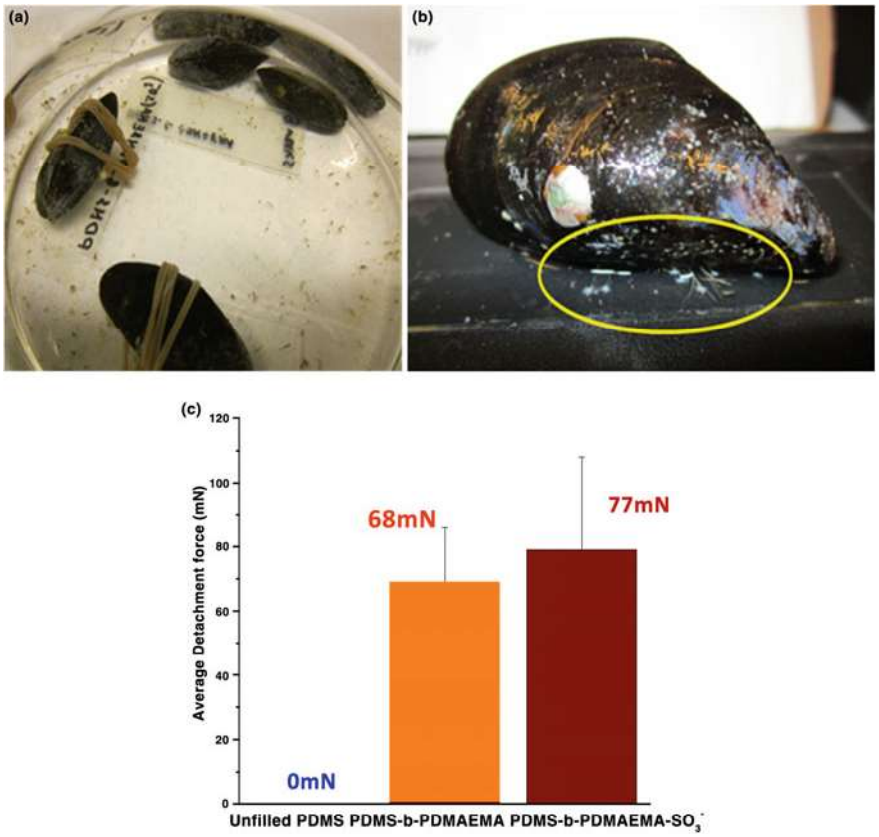

Fig. 15.25 **a** Adhesion experiments with mussels; **b** byssal threads produced onto a block copolymer-filled silicone coating; **c** average detachment forces measured for the two copolymer-filled silicone coatings after 4 weeks immersion in water

surfaces with higher energy (i.e., block copolymer-filled coatings after immersion in water). Although there are controversial opinions in the literature, our results are in good agreement with the studies of Crisp et al. [85] and Waite [54]. Indeed, in these studies, mussels prefer surfaces with higher critical surface energy and their plaques are more strongly attached to slate and glass surfaces than to plastic acetal (acetate), paraffin wax and polytetrafluoroethylene (PTFE) surfaces.

In addition, the chemical aspects related to the attachment of the mussel byssus to the coatings can be explained in terms of biological adhesion. Aquatic surfaces in nature are usually charged and in equilibrium with their environment, populated by an electrical double layer of ions [87]. Surface adsorption of underwater bioadhesives likely occurs by exchange of surface-bound ligands by amino acid sidechains, driven primarily by the relative affinities and effective concentrations of polymeric functional groups. In mussel byssal plaques, two individual adhesive proteins

Mfp-3 and Mfp-5 (Mussel foot proteins) are found at the interface and have been shown to exhibit remarkable binding to surfaces [88]. The versatility of mussel adhesion to surfaces with wide-ranging chemical and physical properties stems from the amino acid 3, 4-dihydroxy-L-phenylalanine (DOPA) but also from the other amino acids which can be hydrophobic, polar or charged. Among the later, phosphorylated serine and lysine residues could be involved in interactions with the PDMS-*b*-PDMAEMA filled coatings and the PDMS-*b*-PDMAEMA-SO_3^- filled coatings, respectively.

15.4 Conclusions

In this work, AFM-based techniques with force sensitivity of a few pN were utilized for mapping the nanostructure and quantifying the nanoscale mechanical properties of the surface of complex polymer coatings based on silicone oligomers in order to use them as bioadhesives. AFM was used in various modes (Peak Force Tapping Mechanical properties and Contact) with different probe tips [Si_3N_4 and chemically-modified tips (CH_3-terminated alkanethiols, COOH-terminated alkanethiols)] both in air and aqueous media.

Nanostructured films of block copolymers containing a polydimethylsiloxane segment and a segment of poly(acrylic acid) or poly((2-dimethylamino) ethyl methacrylate) were investigated. The results have allowed for a better understanding of the interaction of the polymer chains with solvent molecules or chains of another polymer in the self-assembly process. Depending on the copolymer structure, its chemical composition and the solvent, a variety of morphologies, lamellar for PDMS-*b*-PDMAEMA and spherical or cylindrical morphologies for PDMS-*b*-PAA, were obtained through the self-assembly of the copolymer chains. Stiffness mapping by PFT-AFM has allowed identifying the difference in mechanical properties between two polymer constituting blocks The effect of copolymer concentration and solvents on the surface morphologies was also studied in details. The results showed that the micellar morphology is independent of the concentration but dependent on the solvent while the micelle size can be controlled by the concentration. Spherical micelles were always obtained in MeOH and THF/MeOH (1:1) mixture when changing the concentration from 20 to 100 mg/mL). Cylindrical micelles were observed in when THF was used as a solvent as a result of a particular orientation of the PAA cores.

Then, these copolymers were used to modify the surface properties of elastomeric PDMS coatings. The effect of the copolymer on the PDMS surface properties before and after immersion in water was also evaluated by various techniques. Contact angle measurements showed that the block copolymer is not presented on the silicone coatings before immersion in water, but an increase in wettability of the coatings was observed after prolonged immersion in water, as a result of the reorganization of the copolymer chains with the migration of hydrophilic chains on top of the coating surface. Consistently, XPS results indicated the appearance of

peaks typical for the hydrophilic blocks (PAA, PDMAEMA, and PDMAEMA-SO_3^-) at the surface. In addition, AFM-based nano-mechanical testing showed that the surface reorganization significantly affects the morphology and the adhesion properties of the silicone coatings. The observed broadening of the adhesion distribution is believed due to the different interactions between hydrophobic/hydrophilic surfaces and the silicon probe tip in aqueous solution.

The nature of the tip-surface interaction forces was clarified by employing functionalized AFM tips. The adhesion force mapping with hydrophobic tips (CH_3-terminated alkanethiols) for 10 wt% PDMS-*b*-PDMAEMA-filled coatings before and after immersion in water was recorded by using chemical force microscopy. The adhesion force maps showed larger forces for the coatings before immersion, thus confirming that the interaction forces between two hydrophobic surfaces are stronger than those between one hydrophobic and one hydrophilic surface. In addition, the interaction forces between amino groups of the PDMAEMA and COOH-terminated tips were investigated as a function of the pH and the ionic strength of aqueous media. The observation of a plateau in the force curves represents the progressive stretching and continuous desorption of individual copolymer chains from the tip surface. These plateau curves exhibit uniform rupture forces, but variable rupture lengths. Multiple plateaus were observed, reflecting detachment of multiple chains. The dynamic changes of polymer desorption were also reported by recording force curves at various pulling speeds and contact times. The results showed that the plateau frequency decreased with increasing the pulling speed from 100 to 10,000 nm/s, but no variation in plateau force frequency was observed when varying contact time, indicating that the electrostatic interaction bridging the polymer to the tip is a fast process. Furthermore, the adhesion force maps recorded at high ionic strength (in 0.1 M NaCl solution) showed a major decrease in the adhesion frequency and plateau forces, indicating a loss of polyelectrolyte properties.

Bio-adhesion experiments with mussels were then performed on the different types of substrates—unfilled PDMS coatings and PDMS coatings filled with block copolymers. The results revealed that these organisms attach preferably to block copolymer-filled coatings after immersion. In this case, after immersion in water and concomitant molecular reorganization at the top-surface of the copolymer-filled coatings, adhesion of mussels occurs and can be quantified. These observations provided evidence for the significant role played by the selected amphiphilic block copolymers to promote bio-adhesion on surface-treated silicone coatings.

Acknowledgements The work is supported by the ARC BIOMIME project (ARC AUWB-2008-08/12-UMH15), the Science Policy Office of the Belgian Federal Government (Belspo IAP-PAI 7/05 *Functional Supramolecular Systems*—FS2), and Fund for Scientific Research of Belgium (FRS-FNRS). The authors also express their thanks to the European Cooperation in Science and Technology (COST) Action TD0906 (2009–2013): «*Biological Adhesives: from Biology to Biomimetics*». Ph.L., Y.D., and P.F. are Senior Research Associate and Research Directors of FRS-FNRS (Belgium), respectively.

References

1. S.J. Holder, N.A.J.M. Sommerdijk, New micellar morphologies from amphiphilic block copolymers: disks, toroids and bicontinuous micelles. Polym. Chem. **2**, 1018–1028 (2011)
2. L. Zhang, A. Eisenberg, Multiple morphologies of "crew-cut" aggregates of polystyrene-b-poly(acrylic acid) block copolymers. Science **268**, 1728–1731 (1995)
3. L. Zhang, A. Eisenberg, Multiple morphologies and characteristics of "crew-cut" micelle-like aggregates of polystyrene-b-poly(acrylic acid) diblock copolymers in aqueous solutions. J. Am. Chem. Soc. **118**, 3168–3181 (1996)
4. J.-C. Huang, Fabrication of a gecko seta-like structure using polydimethylsiloxane. Int. J. Adhes. Adhes. **36**, 25–31 (2012)
5. D. Xiao, H. Zhang, M. Wirth, Chemical modification of the surface of poly(dimethylsiloxane) by atom-transfer radical polymerization of acrylamide. Langmuir **18**, 9971–9976 (2002)
6. J.C. McDonald, D.C. Duffy, J.R. Anderson, D.T. Chiu, H. Wu, O.J.A. Schueller, G.M. Whitesides, Fabrication of microfluidic systems in poly(dimethylsiloxane). Electrophoresis **21**, 27–40 (2000)
7. X. Ren, M. Bachman, C. Sims, G.P. Li, N. Allbritton, Electroosmotic properties of microfluidic channels composed of poly(dimethylsiloxane). J. Chromatogr. B Biomed. Sci. Appl. **762**, 117–125 (2001)
8. J. Roth, V. Albrecht, M. Nitschke, C. Bellmann, F. Simon, S. Zschoche, S. Michel, C. Luhmann, K. Grundke, B. Voit, Surface functionalization of silicone rubber for permanent adhesion improvement. Langmuir **24**, 12603–12611 (2008)
9. D.T. Eddington, J.P. Puccinelli, D.J. Beebe, Thermal aging and reduced hydrophobic recovery of polydimethylsiloxane. Sens. Actuator B Chem. **114**, 170–172 (2006)
10. D. Bodas, C. Khan-Malek, Formation of more stable hydrophilic surfaces of PDMS by plasma and chemical treatments. Microelectron. Eng. **83**, 1277–1279 (2006)
11. R Kalinova, *Imparting (bio)adhesive properties to silicone coatings: the effect of functionalized diblock copolymers*. Ph.D. Thesis, University of Mons (2013)
12. C. Gerber, H.P. Lang, How the doors to the nanoworld were opened. Nat. Nanotechnol. **1**, 3–5 (2006)
13. A. Engel, D.J. Muller, Observing single biomolecules at work with the atomic force microscope. Nat. Struct. Mol. Biol. **7**, 715–718 (2000)
14. J.K.H. Hörber, M.J. Miles, Scanning probe evolution in biology. Science **302**, 1002–1005 (2003)
15. G. Kada, F. Kienberger, P. Hinterdorfer, Atomic force microscopy in bionanotechnology. Nano Today **3**, 12–19 (2008)
16. M. Chyasnavichyus, S.L. Young, V. Tsukruk, Recent advances in micromechanical characterization of polymer, biomaterial, and cell surfaces with atomic force microscopy. Jpn. J. Appl. Phys. **54**, 08LA02-1-13 (2015)
17. A. Noy, D.V. Vezenov, C.M. Lieber, Chemical force microscopy. Annu. Rev. Mater. Res. **27**, 381–421 (1997)
18. B. Bhushan, O. Marti, in *Handbook of Nanotechnology*, ed. by B. Bhushan (Springer, Heidelberg, 2010), pp. 573–617
19. J Melcher, D Kiracofe, S Hu, A Raman, VEDA 2.0 (Virtual Environment for Dynamic AFM) (2008), http://nanohub.org/resources/adac. doi:10.4231/D38W3821D. Accessed 09 May 2016
20. B.V. Derjaguin, V.M. Muller, Y.P. Toporov, Effect of contact deformations on the adhesion of particles. J. Colloid Interface Sci. **53**, 314–325 (1975)
21. K.L. Johnson, K. Kendall, A.D. Roberts, Surface energy and the contact of elastic solids. Proc. R. Soc. Lond. A **324**, 301–313 (1971)
22. S.A. Chizhik, Z. Huang, V.V. Gorbunov, N.K. Myshkin, V.V. Tsukruk, Micromechanical properties of elastic polymeric materials as probed by scanning force microscopy. Langmuir **14**, 2606–2609 (1998)

23. K.O. van der Werf, C.A.J. Putman, B.G. de Grooth, J. Greve, Adhesion force imaging in air and liquid by adhesion mode atomic force microscopy. Appl. Phys. Lett. **65**, 1195–1197 (1994)
24. S. Seghezza, S. Dante, A. Diaspro, C. Canale, High resolution nanomechanical characterization of multi-domain model membranes by fast force volume. J. Mol. Recognit. **28**, 742–750 (2015)
25. Q. Zhong, D. Inniss, K. Kjoller, V.B. Elings, Fractured polymer/silica fiber surface studied by tapping mode atomic force microscopy. Surf. Sci. Lett. **290**, L688–L692 (1993)
26. P. Leclère, R. Lazzaroni, J.L. Brédas, J.M. Yu, P. Dubois, R. Jérôme, Microdomain morphology analysis of block copolymers by atomic force microscopy with phase detection imaging. Langmuir **12**, 4317–4320 (1996)
27. P. Maivald, H. Butt, S. Gould, C. Prater, B. Drake, J. Gurley, V. Elings, P. Hansma, Using force modulation to image surface elasticities with the atomic force microscopy. Nanotechnology **2**, 103–106 (1991)
28. G. Stan, S.W. King, R.F. Cook, Nanoscale mapping of contact stiffness and damping by contact resonance atomic force microscopy. Nanotechnology **23**, 215703 (2012)
29. D.C. Hurley, M. Kopycinska-Müller, D. Julthongpiput, M.J. Fasolka, D.C. Hurley, M. Kopycinska-Müller, D. Julthongpiput, M.J. Fasolka, Appl. Surf. Sci. **253**, 1274–1281 (2006)
30. U. Rabe, S. Amelio, M. Kopycinska, S. Hirsekorn, M. Kempf, M. Göken, W. Arnold, Imaging and measurement of local mechanical material properties by atomic force acoustic microscopy. Surf. Interface Anal. **33**, 65–67 (2002)
31. R. Arinéro, G. Lévêque, P. Girard, J.Y. Ferrandis, Image processing for resonance frequency mapping in atomic force modulation microscopy. Rev. Sci. Instrum. **78**, 023703-1–023703-6 (2007)
32. B.J. Rodriguez, C. Callahan, S.V. Kalinin, R. Proksch, Dual-frequency resonance-tracking atomic force microscopy. Nanotechnology **18**, 475504 (2007)
33. F. Dinelli, H. Assender, N. Takeda, G. Briggs, O. Kolosov, Elastic mapping of heterogeneous nanostructures with ultrasonic force microscopy (UFM). Surf. Interface Anal. **27**, 562–567 (1999)
34. A. Rosa-Zeiser, E. Weilandt, S. Hild, O. Marti, The simultaneous measurement of elastic, electrostatic and adhesive properties by scanning force microscopy: pulsed-force mode operation. Meas. Sci. Technol. **8**, 1333–1338 (1997)
35. T.J. Young, M.A. Monclus, T.L. Burnett, W.R. Broughton, S.L. Ogin, P.A. Smith, The use of the PeakForceTM quantitative nanomechanical mapping AFM-based method for high-resolution Young's modulus measurement of polymers. Meas. Sci. Technol. **22**, 125703 (2011)
36. G. Stan, R.S. Gates, Intermittent contact resonance atomic force microscopy. Nanotechnology **25**(24), 245702 (2014)
37. M.J. Holzwarth, A.M. Gigler, O. Marti, Digital pulsed force mode—determining local mechanical properties of HeLa cells. Imaging Microsc. **8**, 37–38 (2006)
38. S.N. Magonov, *Expanding Atomic Force Microscopy with HybriD Mode Imaging*. NT-MDT Application Note 087 (2014)
39. C. Braunsmann, J. Seifert, J. Rheinlaender, T.E. Schäffer, High-speed force mapping on living cells with a small cantilever atomic force microscope. Rev. Sci. Instrum. **85**, 073703 (2014)
40. B. Choi, *Park PinPoint™ Mode for Cell Biology* (Private Communication, Boston, MA, 2015)
41. I. Sokolov, *Ringing Mode^{TM}* (Private Communication, Boston, MA, 2015)
42. O. Sahin, S.N. Magonov, C. Su, C.F. Quate, O. Solgaard, An atomic force microscopy tip designed to measure time-varying nanomechanical forces. Nat. Nanotechnol. **2**, 507–514 (2007)
43. S. Jesse, S.V. Kalinin, R. Proksch, A.P. Baddorf, B.J. Rodriguez, The band excitation method in scanning probe microscopy for rapid mapping of energy dissipation on the nanoscale. Nanotechnology **18**, 435503 (2007)

44. D. Platz, E.A. Tholen, D. Pessen, D.B. Haviland, Intermodulation atomic force microscopy. Appl. Phys. Lett. **92**, 153106 (2008)
45. P. Vitry, E. Bourillot, C. Plassard, Y. Lacroute, L. Tetard, E. Lesniewska, Advances in quantitative nanoscale subsurface imaging by mode-synthesizing atomic force microscopy. Appl. Phys. Lett. **105**, 053110 (2014)
46. A. Belianinov, S.V. Kalinin, S. Jesse, Complete information acquisition in dynamic force microscopy. Nat. Commun. **6**, 6550 (2015)
47. C. Chen, J. Wang, Z. Chen, Surface restructuring behavior of various types of poly (dimethylsiloxane) in water detected by SFG. Langmuir **20**(23), 10186–10193 (2004)
48. A. Beigbeder, R. Mincheva, M. Claes, P. Brocorens, R. Lazzaroni, P. Dubois, On the effect of carbon nanotubes on the wettability and surface morphology of hydrosilylation-curing silicone coatings. J. Nanostruct. Polym. Nanocompos. **5**, 37–43 (2009)
49. R. Kalinova, R. Mincheva, P. Dubois, Imparting adhesion property to silicone materials: challenges and solutions. Rev. Adhes. Adhes. **2**, 30–55 (2014)
50. I. Marabotti, A. Morelli, L.M. Orsini, E. Martinelli, G. Galli, E. Chiellini, E.M. Lien, M.E. Pettitt, M.E. Callow, J.A. Callow, S.L. Conlan, R.J. Mutton, A.S. Clare, A. Kocijan, C. Donik, M. Jenko, Fluorinated/siloxane copolymer blends for fouling release: chemical characterisation and biological evaluation with algae and barnacles. Biofouling **25**, 481–493 (2009)
51. E. Martinelli, M.K. Sarvothaman, G. Galli, M.E. Pettitt, M.E. Callow, J.A. Callow, S.L. Conlan, A.S. Clare, A.B. Sugiharto, C. Davies, D. Williams, Poly(dimethyl siloxane) (PDMS) network blends of amphiphilic acrylic copolymers with poly(ethylene glycol)-fluoroalkyl side chains for fouling-release coatings. II. Laboratory assays and field immersion trials. Biofouling **28**, 571–582 (2012)
52. H. Lee, B.P. Lee, P.B. Messersmith, A reversible wet/dry adhesive inspired by mussels and geckos. Nature **448**, 338–341 (2007)
53. J.H. Waite, Nature's underwater adhesive specialist. Int. J. Adhes. Adhes. **7**, 9–14 (1987)
54. J.H. Waite, Adhesion a la moule. Integr. Comp. Biol. **42**, 1172–1180 (2002)
55. L. Leibler, Theory of microphase separation in block copolymers. Macromolecules **13**, 1602–1617 (1980)
56. J.H. Hildebrand, R.L. Scott, *The Solubility of Non-electrolytes*, 3rd edn. (Reinhold, New York, 1975)
57. Z. Tuzar, P. Kratochvíl, Block and graft copolymer micelles in solution. Adv. Colloid Interface Sci. **6**, 201–232 (1976)
58. J.H. Hildebrand, R.L. Scott, *ReguZar Solutions* (Prentice-Hall, Englewood Cliffs, 1962)
59. J.H. Hildebrand, J.M. Prausnitz, R.L. Scott, *Regular and Related Solutions* (van Nostrand-Reinhold, Princeton, NJ, 1970)
60. C. Price, in *Developments in Block Copolymers*, ed. by I. Goodman (Applied Science Publishers, Barking, 1982), pp. 39–79
61. J.G. Selb, Y. Gallot, in *Developments in Block Copolymers*, vol. 2, ed. by I. Goodman (Applied Science Publishers, London, 1985), p. 327
62. Z. Tuzar, P. Kratochvil, in *Surface and Colloid Science*, vol. 15, ed. by E. Matijevic (Plenum Press, New York, 1993), pp. 1–83
63. O. Dos Santos Ferreira, E. Gelinck, D. de Graaf, H. Fischer, Adhesion experiments using an AFM—parameters of influence. Appl. Surf. Sci. **257**, 48–55 (2010)
64. R. Kalinova, C. Ngo, R. Mincheva, R. Lazzaroni, P. Leclère, P. Dubois, From cylindrical to spherical nanosized micelles by self-assembly of poly(dimethylsiloxane)-b-poly(acrylicacid) diblock copolymers. Polym. Bull. (2015). doi:10.1007/s00289-016-1598-2
65. M.-E. Vlachopoulou, A. Tserepi, K. Beltsios, G. Boulousis, E. Gogolides, Nanostructuring of PDMS surfaces: dependence on casting solvents. Microelectron. Eng. **84**, 1476–1479 (2007)
66. L.B. Thiele, R. Frommelt, H. Faserforschung, Z. Textiltechnik, Polymerforschung **28**, 405 (1977)
67. J.N. Israelachvili, P.M. McGuiggan, Forces between surfaces in liquids. Science **241**, 795–800 (1988)

68. E.E. Meyer, K.J. Rosenberg, J. Israelachvili, Recent progress in understanding hydrophobic interactions. Proc. Natl. Acad. Sci. USA **103**, 15739–15746 (2006)
69. D. Alsteens, E. Dague, P.G. Rouxhet, A.R. Baulard, Y.F. Dufrêne, Direct measurement of hydrophobic forces on cell surfaces using AFM. Langmuir **23**, 11977–11979 (2007)
70. A. Beigbeder, M. Jeusette, R. Mincheva, M. Claes, P. Brocorens, R. Lazzaroni, P. Dubois, On the effect of carbon nanotubes on the wettability and surface morphology of hydrosilylation-curing silicone coatings. JNPN **5**, 37–43 (2009)
71. E. Duquesne, J. Habimana, P. Degée, P. Dubois, Synthesis of silicone-methacrylate copolymers by ATRP using a nickel-based supported catalyst. Macromol. Chem. Phys. **207**, 1116–1125 (2006)
72. T.C. Ngo, R. Kalinova, D. Cossement, E. Hennebert, R. Mincheva, R. Snyders, P. Flammang, P. Dubois, R. Lazzaroni, Ph Leclère, Modification of the adhesive properties of silicone-based coatings by block copolymers. Langmuir **30**, 358–368 (2013)
73. E.W. van der Vegte, G. Hadziioannou, Acid–base properties and the chemical imaging of surface-bound functional groups studied with scanning force microscopy. J. Phys. Chem. B **101**, 9563–9569 (1997)
74. J.N. Israelachvilli, *Intermolecular and Surface Forces* (Academic Press, New York, 1992)
75. T. Hugel, M. Seitz, The study of molecular interactions by AFM force spectroscopy. Macromol. Rapid Commun. **22**, 989–1016 (2001)
76. B. Cappella, G. Dietler, Force-distance curves by atomic force microscopy. Surf. Sci. Rep. **34**, 1–104 (1999)
77. R. Barattin, N. Voyer, Chemical modifications of AFM tips for the study of molecular recognition events. Chem. Commun. **13**, 1513–1532 (2008)
78. C. Jérôme, N. Willet, R. Jérôme, A.S. Duwez, Electrografting of polymers onto AFM tips: a novel approach for chemical force microscopy and force spectroscopy. Chem. Phys. Chem. **5**, 147–149 (2004)
79. C. Friedsam, M. Seitz, H.E. Gaub, Investigation of polyelectrolyte desorption by single molecule force spectroscopy. J. Phys. Condens. Matter **16**, S2369–S2382 (2004)
80. J.H. Waite, Adhesion in byssally attached bivalves. Biol. Rev. **58**, 209–231 (1983)
81. R. Merkel, P. Nassoy, A. Leung, K. Ritchie, E. Evans, Energy landscapes of receptor–ligand bonds explored with dynamic force spectroscopy. Nature **397**, 50–53 (1999)
82. M. Rief, M. Gautel, F. Oesterhelt, J.M. Fernandez, H.E. Gaub, Reversible unfolding of individual titin immunoglobulin domains by AFM. Science **276**, 1109–1112 (1997)
83. D. Alsteens, C.B. Ramsook, P.N. Lipke, Y.F. Dufrêne, Unzipping a functional microbial amyloid. ACS Nano **6**, 7703–7711 (2012)
84. M.A. Nash, H.E. Gaub, Single-molecule adhesion of a stimuli-responsive oligo(ethylene glycol) copolymer to gold. ACS Nano **6**, 10735–10742 (2012)
85. D.J. Crisp, G. Walker, G.A. Young, A.B. Yule, Adhesion and substrate choice in mussels and barnacles. J. Colloid Interface Sci. **104**, 40–50 (1985)
86. N. Aldred, L.K. Ista, M.E. Callow, J.A. Callow, G.P. Lopez, A.S. Clare, Mussel (*Mytilus edulis*) byssus deposition in response to variations in surface wettability. J. R. Soc. Interface **3**, 37–43 (2006)
87. R.J. Stewart, T.C. Ransom, V. Hlady, Natural underwater adhesives. J. Polym. Sci. Part B Polym. Phys. **49**, 757–771 (2011)
88. J. Yu, Y. Kan, M. Rapp, E. Danner, W. Wei, S. Das, D.R. Miller, Y. Chen, J.H. Waite, J.N. Israelachvili, Adaptive hydrophobic and hydrophilic interactions of mussel foot proteins with organic thin films. Proc. Natl. Acad. Sci. USA **110**, 15680–15685 (2013)
89. A.F.M. Barton, Solubility parameters. Chem. Rev. **75**(6), 731–753 (1975)
90. S. O'Driscoll, G. Demirel, R.A. Farrell, T.G. Fitzgerald, C. O'Mahony, J.D. Holmes, M.A. Morris, The morphology and structure of PS-b-P4VP block copolymer films by solvent annealing: effect of the solvent parameter. Polym. Adv. Technol. **22**, 915–923 (2011)
91. J. Brandrup, E.H. Immergut, E.A. Grulke (eds.), *Polymer Handbook*, 4th edn. (Wiley, New York, 1999)